ALL-OPTICAL METHOD FOR DISTORTION ELIMINATION IN PHASE-MODULATED MICROWAVE PHOTONIC LINKS

by
Amit Bhatia

A dissertation submitted to Johns Hopkins University in conformity with the requirements for the degree of Doctor of Philosophy

Baltimore, Maryland
January 2017

Abstract

Microwave photonic systems arose from the need to accomplish engineering goals that were not possible in the electrical domain alone. One of the first applications of photonic systems was in long haul microwave signal transport, leveraging the wide bandwidth and low propagation loss afforded by optical fiber. As these microwave photonic links became more widespread, so too did the efforts to improve their performance, most importantly the desire to minimize noise and distortion within the link in order to maximize dynamic range and linear performance. In this thesis, we demonstrate a new class of methods for microwave photonic link linearization that connects insights from a seemingly unrelated field- nonlinear optics- with microwave photonics to enhance the distortion-free operation of these links. Finally, we show applications for these methods in other areas of microwave photonics, particularly microwave signal generation.

Table of Contents

Table of Figures

1 Introduction

In this thesis we introduce a novel method for distortion elimination in phase-modulated microwave photonic links. Though there are many other distortion elimination methods, they all use electronics or electro-optics to accomplish the linearization. The method we have developed resides in a class by itself. That is, it accomplishes the linearization entirely in the optical domain, something that has not been done before. This introduction lays the groundwork for understanding this method by giving a brief overview of microwave photonics, including various types of links, their pertinent metrics, and tradeoffs between them, and nonlinear optics, including four-wave mixing (FWM) and stimulated Brillouin scattering (SBS), the two most significant nonlinear optical processes present in the design. Chapter two focuses on the theory of operation for our method. Chapters three and four describe our implementation as well as results we have obtained. Chapter five discusses operational issues, limitations, and tradeoffs of this design. Finally chapter 6 discusses another potential application of this method, microwave function generation, including our design and experimental results.

1.1 Microwave Photonics

Microwave photonics, a subfield of microwave and optical engineering, involves the optical generation, processing, or transmission of analog

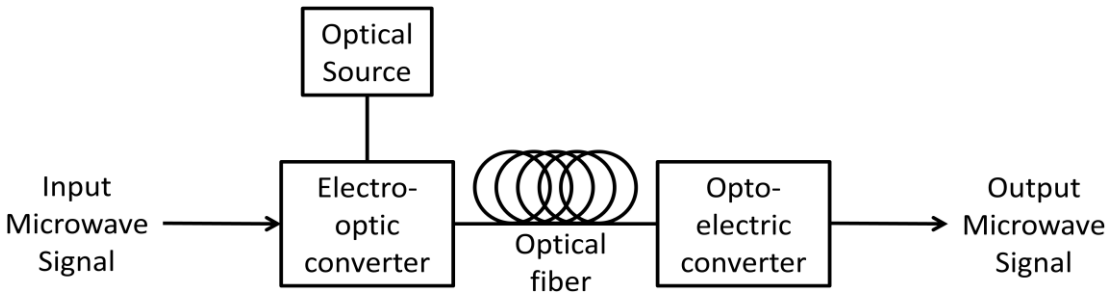

Figure 1.1 The key components of a microwave photonic system: an optical source, an electro-optic converter, optical fiber, and an opto-electric converter.

electrical signals. The key components of a microwave photonic system are an optical source, a method of fast modulation, suitable transmission media, and a fast detector (see Fig. 1.1). Initial work on microwave photonics began as soon as the laser was invented in 1960 at the Hughes Research Labs [1]. The subsequent development of electro-optic modulators capable of gigahertz modulation, low loss silica single-mode fibers, and fast-depletion PIN and avalanche photodetectors served to spur the field further. This along with its advantages of high bandwidth, low and constant attenuation over the microwave modulation frequency range, small size, low weight, low cost, low dispersion, and immunity to electromagnetic interference, have made microwave photonic systems attractive alternatives in numerous domains traditionally reserved for transmission line electronics. These include distribution of CATV signals, antenna remoting, radio-over-fiber links, true-time delay beamforming for phased-array antennas, and photonic analog-to-digital conversion [1-6].

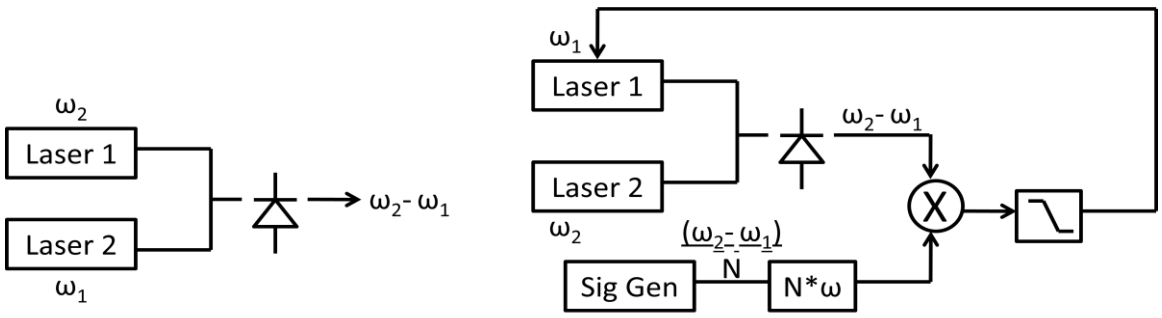

Figure 1.2 (left) Two free-running lasers create a beat note at a photodetector at a microwave frequency that is the difference between the two laser frequencies; (right) an optical phase locked loop.

1.1.1 Microwave Photonic Generation

Microwaves are photonically generated by creating a beat note at a photodetector between two lasers, separated in frequency by the desired microwave frequency (see Fig. 1.2). However, if the two lasers are free-running, the microwave signal would have high phase noise because the phase terms of the optical signals are not correlated and the beating process will transfer the phase noise of the optical waves to the microwave signal. As a result, multiple methods have been explored to phase lock the two lasers together. A simple method is to low bias an intensity modulator and drive it with a microwave signal at half the desired frequency. By beating the two first order sidebands together, a microwave signal at twice the input microwave frequency is produced. Other techniques like optical injection locking and optical phase-locked loops have also been tried. For a more detailed discussion, the interested reader is referred to [2].

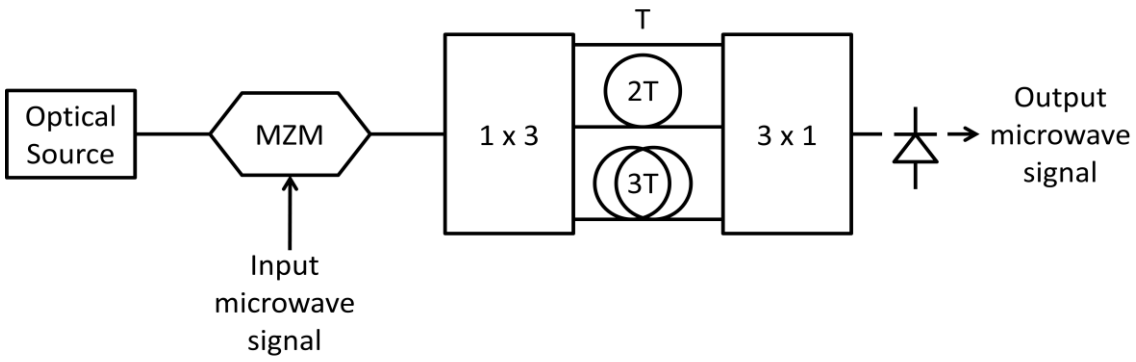

Figure 1.3 A three-tap microwave photonic delay-line filter. An input microwave signal is split in a 1x3 coupler and each branch is scaled (not shown) and delayed a different amount with a fundamental delay of T. The output signal is a filtered version of the input.

1.1.2 Microwave Photonic Processing

Microwave signal processing can be accomplished in a myriad of ways. Here, we discuss microwave photonic delay-line filtering, analog-to-digital conversion, and waveform generation. Delay-line filtering is an example of FIR filtering and works by adding together delayed, scaled copies of the original signal (see Fig. 1.3). The fundamental delay T is the inverse of the free spectral range (FSR) of the filter. Because optical intensity can only be positive, in the simplest architectures, the scale factors can only be positive. However, since only low-pass filtering can be accomplished with positive tap coefficients, much effort has been devoted to producing negative and complex coefficients in order to realize band-pass filtering. A few ways to produce negative tap coefficients include using differential detection to perform the subtraction electronically, using opposing slopes of the

modulator response, and utilizing phase modulation and linearly chirped fiber Bragg gratings. Complex coefficients can be implemented with nonuniformly spaced taps [2].

Analog-to-digital conversion (ADC) can also be accomplished in many ways. A photonic ADC can be defined as a device with an analog electronic input and a digital electronic output that uses photonics in the digitization process. These devices can be classified as photonic assisted, photonic sampled, photonic quantized, and photonic sampled and quantized. A detailed discussion is beyond the scope of this work but the interested reader is referred to [7] and [8], which provide a thorough overview of the subject.

Arbitrary waveform generation can be realized in a multitude of ways. One way is to spectrally disperse a supercontinuum source with a diffraction grating, shape the pulse with a high resolution spatial light modulator (SLM), focus all the spectral components onto a dispersive optical fiber, and finally detect it at a photodiode [3]. The pattern etched by the SLM becomes the electrical signal in the time domain. In Chapter 6, we explain an alternate method for microwave function generation that leverages the techniques we develop in this thesis.

1.1.3 Microwave Photonic Transmission

The majority of this thesis is devoted to microwave photonic transmission

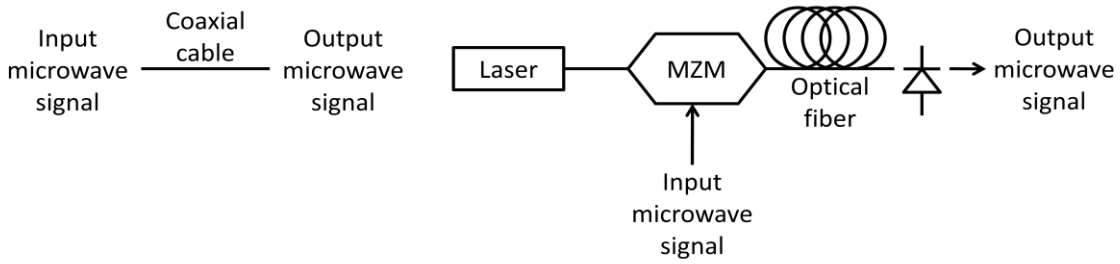

Figure 1.4 (left) A coaxial link; (right) an intensity modulated direct detection photonic link.

and linearization (processing) of those communication links. Accordingly, we devote the majority of the introduction to this section. We give a brief overview of various types of links, relevant link metrics, tradeoffs between these metrics, and previous methods of link linearization.

1.1.3.1 Link Types

Communication links can come in many different incarnations. In this section we summarize photonic vs coaxial links, analog vs digital links, directly modulated vs externally modulated links, and intensity vs phase modulated links.

1.1.3.1.1 Photonic Links vs Coaxial Links

Though the propagation loss of optical fiber is much lower and more uniform over frequency relative to coaxial cables, it does present high electro-optic conversion loss. In order to justify this loss, incurred by transferring

back and forth between the electrical and optical domains, optical fiber must provide sufficient advantages over coax (see Fig. 1.4). These advantages have been mentioned earlier and in [1-6]. Generally, the higher the bandwidth length product of the link, the more beneficial it is to shift to a photonic link. That is, because of the low and flat attenuation over microwave modulation bandwidths and the low propagation loss, traversing enough distance with enough information allows the link to overcome the electro-optic conversion losses thereby posing an advantage over a coaxial link. This work focuses on photonic links.

1.1.3.1.2 Analog Links vs Digital Links

The data transmitted by the communication link can be transmitted in either the analog or digital domain. This work focuses on the analog domain. Digital communications depend on (in the simplest case) the receiver's ability to distinguish between two states (e.g. two optical power levels) rather requiring an accurate reproduction of an infinite number of states as is the case with analog communications. Thus digital signals are more fault tolerant while analog signals are more susceptible to noise and distortion introduced by the channel or devices within the link. Significantly, digital signals can be regenerated via regularly spaced repeaters, thus allowing theoretically infinite transmission distance without information loss and minimal impact to bit error rates (BER). By contrast, once an analog signal

is created, its signal-to-noise ratio (SNR) continuously degrades and can never be restored. The invention of the erbium-doped fiber amplifier (EDFA) in the 1980s enabled practical digital communication systems by allowing signals to be transmitted over much longer distances before requiring regeneration. Though this also aided in analog signal transmission, noise introduced by the EDFA degraded the SNRs. While the majority of optical communication is digital, there are many niche applications for analog communications, including the distribution of CATV signals, subcarrier multiplexing, radar beamforming, radio over fiber, and antenna remoting [1-6]. In addition, as higher order modulation formats continue to be adopted in the digital domain, digital links begin to look increasingly analog and thus analog performance metrics become relevant.

1.1.3.1.3 Direct Modulation vs External modulation

Direct modulation involves directly modulating the current driving the laser source with the electronic signal. External modulation involves using a separate device, an electro-optic modulator, which allows an additional degree of freedom so that the laser specifications can be chosen independently of the modulation requirements. Direct modulation has greater RIN and introduces chirp. This work focuses on external modulation.

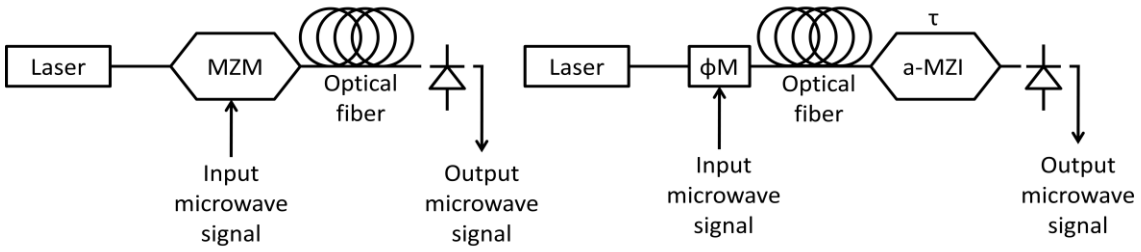

Figure 1.5 (left) An intensity modulated direct detection (IMDD) photonic link; (right) a phase modulated interferometrically detected (ΦMID) link.

1.1.3.1.4 IMDD Links vs ΦMID Links

Analog links can modulate the carrier lightwaves' intensity, frequency, phase, or polarization. Of the analog link architectures, the simplest and most common is the intensity-modulated directly-detected (IMDD) link (see Fig. 1.5). In this architecture, the input microwave signal modulates the intensity of a lightwave via an external Mach-Zehnder modulator (MZM), then travels through an optical fiber span to a photodetector, which recovers the original microwave signal. Because photodetectors can only convert intensity fluctuations into current fluctuations, the latter three types of modulation formats must be converted to intensity fluctuations via an optical local oscillator or an interferometer prior to detection. For reasons that will become clear, in this thesis we focus on phase-modulated interferometrically-detected (ΦMID) links in which the phase of the lightwave is modulated by the microwave signal. The lightwave travels through an optical fiber span to a receiver containing an asymmetric Mach-Zehnder interferometer (a-MZI), which performs the phase to intensity conversion, and then to a balanced

photodetector, where the original signal is recovered (see Fig. 1.5).

ΦMID links have several distinct advantages over IMDD links including a simpler transmit end that does not require active biasing, which is beneficial when the transmit end is resource limited such as in antenna remoting. However, this transmitter simplicity comes at the cost of receiver complexity. Secondly, ΦMID links have the ability to perform balanced detection without needing to run a dual path-matched fiber span. Thirdly, electro-optic phase modulation has a high degree of linearity in the phase modulation process. Thus optical signal processing methods have access to nearly distortion-free phase modulated signals because distortion does not enter the link until the interferometric receiver. Finally, ΦMID links offer greater gain, lower noise figure, and higher SFDR at the cost of reduced bandwidth. Detailed performance tradeoffs can be found in [9].

1.1.3.2 Link Metrics

Like any other active device, microwave photonic links can be characterized by four main performance metrics: gain, noise figure (NF), bandwidth, and spurious-free dynamic range (SFDR) [10]. Often gain and bandwidth are measured simultaneously via an S21 scattering parameter measurement for a two-port device on an electronic network analyzer (see Fig. 1.6).

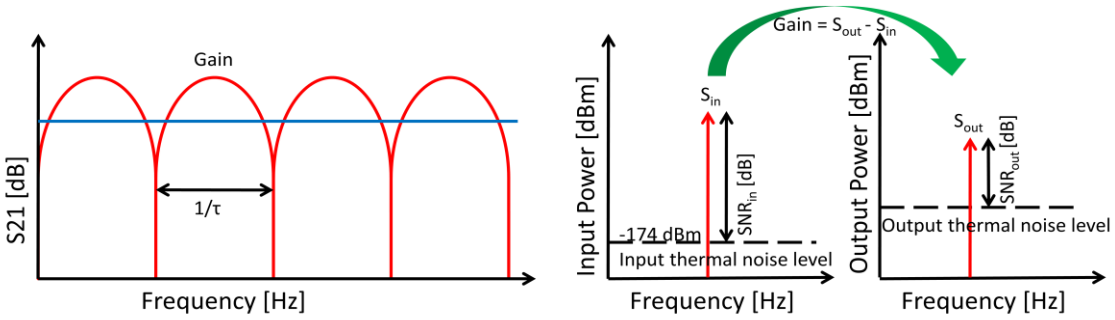

Figure 1.6 (left) Gains of an IMDD link (in blue) and a ΦMID link (in red); (right) SNRs at the input and output of a link. The noise figure (NF) can be computed by taking the difference between the input and output SNRs.

1.1.3.2.1 Noise Figure

Noise figure is a quantity that describes the amount of noise added by the link (see Fig. 1.6). Noise is a deep topic and a full discussion is beyond the scope of this thesis. Here we touch on the major concepts and provide references [11-14] for the interested reader. In a passive coaxial link the NF equals the loss. In a photonic link, however, noise is added from a multitude of additional sources including thermal noise, shot noise, and relative intensity noise (RIN). If optical amplifiers are used then amplified spontaneous emission (ASE) noise also contributes and depending on the method of modulation, laser phase noise may also play a role. Thermal noise is produced in the resistive parts of the link by the random, temperature-induced motion of electrons and holes and is independent of current in the photodetector [11, 12]. Shot noise is caused by current fluctuation in the photodetector due to the quantum nature of electrons and is directly

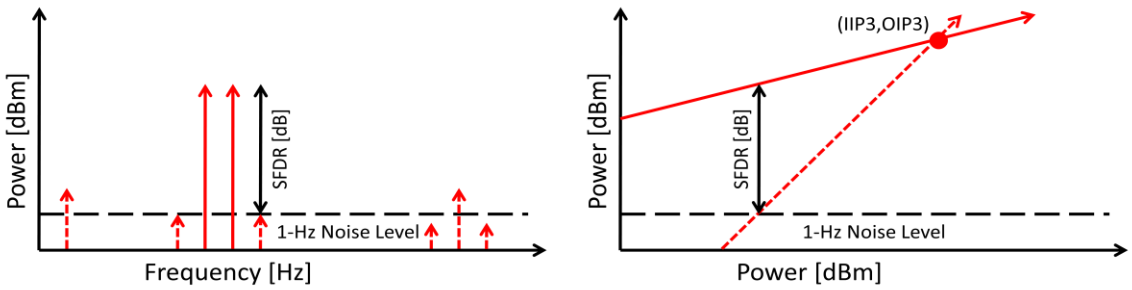

Figure 1.7 (left) In a two-tone test of a link, the spurious-free dynamic range (SFDR) is the magnitude of the fundamentals above the 1-Hz noise floor when the 3rd order distortion products just touch the noise floor; (right) The SFDR can also be calculated by sweeping the input power of the link and measuring the fundamental and 3rd order distortion tone.

proportional to the photodetector current [13, 14]. RIN is caused by the spontaneous emission of photons by the laser and is proportional to the square of the photodetector current. As a point of reference, for photocurrents less than 1 mA, thermal noise typically dominates, for photocurrents above 100 mA, RIN typically dominates, and for photocurrents between these values, links typically operate in the shot noise limited regime [15-17]. Laser phase noise can be compounded and redistributed by optical amplification, dispersive elements, and nonlinear processes within the link.

1.1.3.2.2 SFDR

SFDR is the range of electrical power that can transmitted through the link (see Fig. 1.7). On the low end it is limited by the noise of the system and on the high end it is limited by the nonlinearity of the system. A signal that

is below the noise floor will be too weak to be detected and a signal that is too strong will produce distortion products that could make the original signal unrecoverable at the output.

1.1.3.2.3 Miscellaneous Metrics

Additional metrics sometimes included in link analysis are compression dynamic range (CDR), receiver sensitivity, and maximum frequency of operation. CDR is defined as the input power for which the theoretically extended fundamental tone exceeds the experimentally measured saturated fundamental tone by 1 dB. Receiver sensitivity is fully determined by the NF and a required signal-to-noise ratio (SNR) at the receiver. Maximum frequency of operation may be device limited or system limited if some type of signal processing is performed within the link. Since CDR and receiver sensitivity are just different measures of distortion and noise, we ignore them and only consider frequency of operation. At some point in the course of link design, the engineer will inevitably ask: given all the relevant metrics for two separate devices, is it possible to derive the metrics of the system, that is, the metrics of the two devices cascaded together. The answer is yes and no. Gain can be cascaded in a relatively straightforward way by adding the individual gains in the decibel domain. If no exotic signal processing occurs in the link, bandwidth can be calculated as the intersection of the bandwidths of the devices. Noise Figure can be

cascaded using the individual gains and the Friis noise formula. However, though there are ways of cascading OIP3 point, there is no straightforward or reliable way of cascading SFDR [6].

1.1.3.3 Tradeoffs between Link Metrics

Optimization of one link metric often comes at the expense of the performance of another. The simplest example of this is the gain-bandwidth tradeoff between phase-modulated and intensity-modulated links [9]. Another is low-biasing to trade higher gain for better noise figure [18]. There are many more tradeoffs detailed in the literature (e.g. chapter 7 of [18]). In this thesis, we demonstrate a novel method for increasing SFDR at a minimal intrinsic cost of gain and noise figure. Though the small reduction in gain is fundamental to this method, the increase in noise figure that we observe is not and can be alleviated by methods that will be discussed in chapter 5.

1.1.3.4 Previous Methods for Link Improvement

Because microwave photonic links form the core of photonic system architectures, there has been much interest in improving link metrics. To improve gain or bandwidth, for example, typically improvements in devices are sought in order to increase their bandwidths, optical power handling capabilities, or reduce their V_π (electro-optic modulator). To improve SFDR, either the NF must be improved or distortions must be eliminated, thus

making the link more linear. Link characteristics are normally fully determined by the devices chosen. However, link linearization is one of the few ways the link designer can improve a link through intelligent system engineering.

1.1.3.4.1 Noise Reduction Techniques

The noise floor is determined by the gain and noise figure of the link [19]. The simplest method of increasing gain and reducing noise figure is to choose a low V_π modulator and a high current photodetector and maximize the optical power while remaining in shot noise limited regime [20, 21]. Due to other constraints, however, we may be limited in the components we can choose and thus require other methods of noise reduction. In [22] the authors compare the effects of balanced detection and low biasing on noise figure using a low V_π modulator, high power photodiodes, and high power low RIN laser source. Balanced detection (see Fig. 1.8) cancels RIN as long as the two arms are of equal length. Low biasing (see Fig. 1.8) the modulator reduces the optical power and therefore both the shot noise and the RIN faster than the slope efficiency, thus increasing the signal to noise ratio (SNR). However, lowering the shot noise to below the thermal noise degrades the performance, so there is an optimum bias point for maximizing SNR [23]. In [24] both low biasing and carrier suppression via delay line optical filtering are explored. By using a balanced modulation and detection scheme in [25], the authors

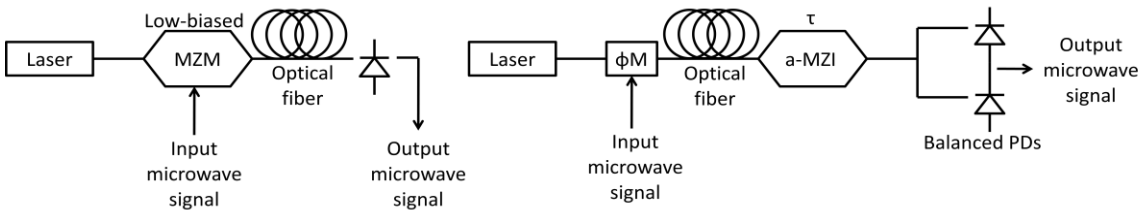

Figure 1.8 (left) Low-biased IMDD link; (right) ΦMID link with balanced detection.

show that the noise currents for the architecture is substantially lower than for a traditional IMDD link. A brief summary of some additional methods is provided in [26].

1.1.3.4.2 Distortion Reduction Techniques

Distortion typically enters a link via the nonlinear transfer function of the interferometric components. It can also be introduced by the fiber, the amplifier, and the photodiode, but these effects are ignored here. The transfer functions (input voltage to output voltage) for both the IMDD and ΦMID links (MZM and a-MZI) are raised cosine functions. When biased at the inflection point (quadrature), all even-order distortions cancel but all odd-order distortions remain. In sub-octave links, third-order distortion is the primary limitation of SFDR. In addition to limiting SFDR, odd-order distortions cause cross-talk among adjacent channels in, for example, a subcarrier multiplexed system and thus it is desirable to eliminate them. Following the notation of [27], the fundamental tones, the 2nd, and the 3rd

order nonlinearities are:

$$I = aV + bV^2 + cV^3$$

$$V = V_1 \cos \omega_1 t + V_2 \cos \omega_2 t$$

$$I_1 = aV_1 \cos \omega_1 t + aV_2 \cos \omega_2 t$$

$$I_2 = \frac{1}{2} b(V_1^2 \cos 2\omega_1 t + V_2^2 \cos 2\omega_2 t + 2V_1 V_2(\cos(\omega_1 + \omega_2)t + \cos(\omega_1 - \omega_2)t) + \cdots)$$

$$I_3 = \frac{1}{2} c(3V_1^2 V_2(\cos(2\omega_1 - \omega_2)t + 3V_1 V_2^2 \cos(2\omega_2 - \omega_1)t) + \cdots)$$

The order of the nonlinearity (sum of the exponents) determines the slope of the nonlinearity and the coefficients determine the intercept on a log-log transfer function plot.

1.1.3.4.2.1 Distortion Reduction Techniques: IMDD Links

Link linearization efforts all involve introducing a small amount of nonlinearity that cancels the distortion with ideally minimal impact to signal gain. However, most of these efforts have been directed toward IMDD links due to their greater ubiquity. Various schemes have been proposed for both IMDD and ΦMID links to reduce distortion and generally fall into one of three categories depending on how the cancelling nonlinearity is implemented: analog electronic (feedback/feedforward) [28-31], digital signal processing [32, 33, 34, 35], and electro-optic [36-40, 41, 42]. One example of electronic distortion elimination is predistortion, in which a microwave signal with equal and opposite nonlinearity to the transfer function is fed into the

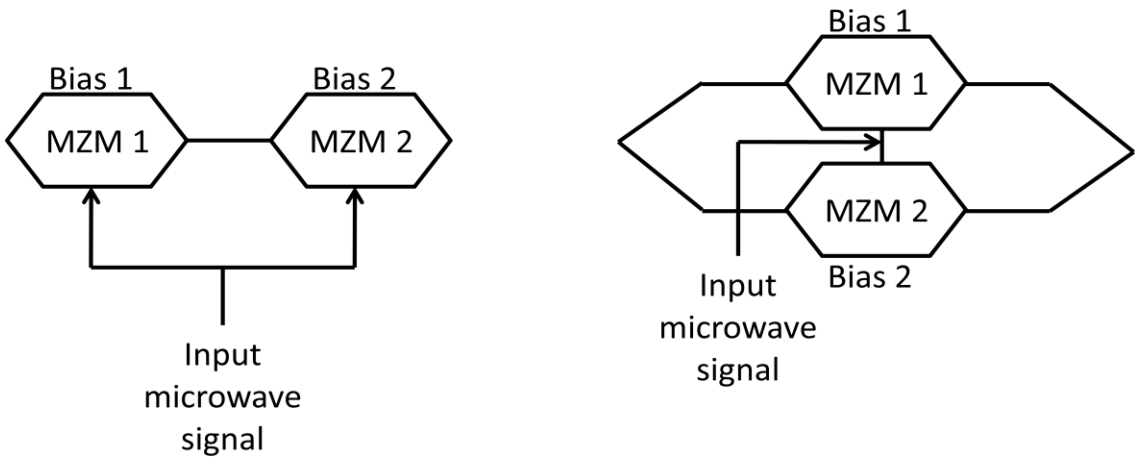

Figure 1.9 (left) Dual series MZM; (right) Dual parallel MZM.

modulator [28, 29]. Another example is feed-forward, in which part of the optical output is detected and compared with the input microwave signal to generate an error signal [30, 31]. This error signal is inverted and sent to a second electro-optic modulator whose output is added to the first output to produce a more linear output. These are costly and complex solutions that requires electronics that can be bandwidth limiting. The second type of distortion elimination involves detecting the output, sending it through an analog-to-digital converter, and using digital signal processing (DSP) to electronically correct the signal [32, 33]. This also requires additional electronics and is inherently bandwidth limited due to the need to directly sample the distorted signals at high rates.

The third type involves connecting multiple modulators or multiple interferometric detectors in either series or parallel (see Fig. 1.9) or otherwise

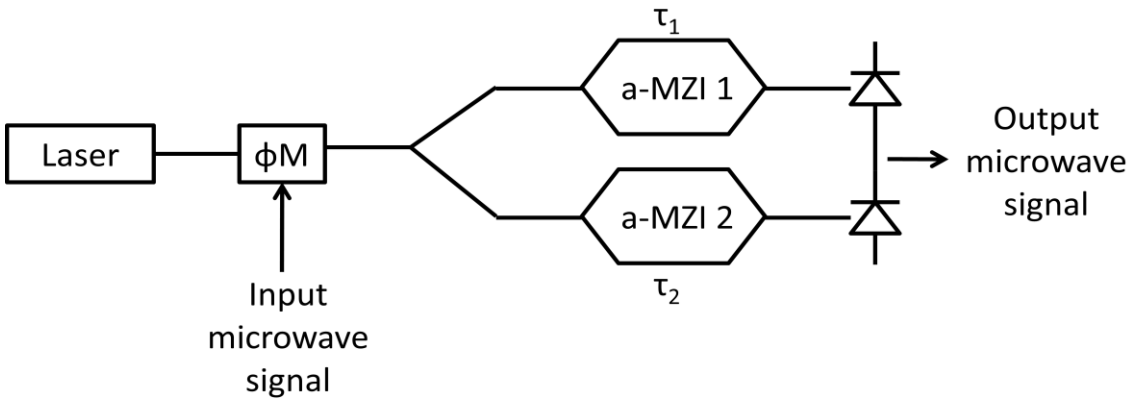

Figure 1.10 Linearized ΦMID link using two a-MZIs and balanced photodetection.

modifying the interferometer in the modulator or detector to produce an output that is more linear than a conventional single MZM [39, 40]. For example, this usually means driving one modulator with a high optical power and low microwave power (low distortion) and the other with low optical power and high microwave power (high distortion), then combining the signals such that the distortion products cancel while the signal does not [36-40]. This is not only environmentally sensitive, but also hardware inefficient as it requires one additional modulator for each additional distortion product cancellation and is thus limited in the amount of practically achievable linearization orders.

1.1.3.4.2.2 Distortion Reduction Techniques: ΦMID Links

Of these methods only [41], [42], [43], and [44] apply to phase-modulated links. In [41, 44], the anisotropy of lithium niobate is exploited to

modulate two orthogonally polarized fields to different depths, effectively creating parallel modulators to cancel third-order distortion. In [42, 43], two actual parallel a-MZIs are used to accomplish the same thing (see Fig. 1.10). All three of these methods are the ΦMID analogue of using two parallel MZMs to linearize an IMDD link as in [37].

In [45] we introduced a fourth linearization category: all-optical, and we experimentally demonstrated all-optical linearization of a phase modulated microwave photonic link. In this method, we tap off a small portion of the phase-modulated signal to seed a cascaded FWM process in an optical comb generator (OCG). The generated lightwaves bear a fixed integer phase relationship with the signal lightwave. By appropriately filtering, scaling, and re-combining one or more of these lightwaves with the original lightwave, we can cancel one or more distortion products and in [45] we demonstrated full cancellation of third-order distortion. In [46], we extend our previous approach to show simultaneous third-order and fifth-order distortion cancellation. We believe that was the first demonstration of simultaneous third-order, fifth-order, and all even-order distortion cancellation in either an intensity or phase modulated microwave photonic link. We explain this method in greater detail in the next chapter.

1.2 Nonlinear Optics

Nonlinear optics is the study of the modification of the optical properties of matter due to the presence of light [47]. In fact, the beginning of this field is typically marked by the discovery of second harmonic generation (SHG) by Franken et al. in [48] by applying an "intense beam of 6934A light through crystalline quartz." Since then, nonlinear processes have been found to be responsible for a host of interesting observable phenomena including sum frequency generation (SFG), difference frequency generation (DFG), second harmonic generation (SHG), the Kerr effect, four-wave mixing (FWM), and stimulated Brillouin scattering (SBS), just to name a few. Here, we restrict ourselves to the consideration of the two nonlinear processes that primarily affect our system: FWM and SBS. In our system, we seek to maximize and exploit the former and minimize the impact of the latter.

1.2.1 Four-Wave Mixing

One class of nonlinear responses is parametric, meaning no energy is exchanged between the light and the medium. So, the total light energy before and after entering the medium, is conserved. Physically the response is caused by the anharmonic motion of bound electrons within the medium. It is mediated by the nonlinear susceptibility and manifests through the

refractive index and absorption coefficient [49]. Within the linear regime, the polarization density increases in proportion with the applied electric field:

$$\mathbf{P} = \chi^{(1)}\mathbf{E}$$

Here, $\chi^{(1)}$ is the linear susceptibility. In the nonlinear regime, however, we must express the polarization density as a power series in the electric field.

$$\mathbf{P} = \chi^{(1)}\mathbf{E} + \chi^{(2)}\mathbf{EE} + \chi^{(3)}\mathbf{EEE} + \cdots$$

Now, if we impose two electric fields on the optical media at high intensity, we can predict the relevant frequencies we would expect at the output following the notation of [47]:

$$\mathbf{E_{in}} = \mathbf{E_1} + \mathbf{E_2} = \mathrm{E}_1 e^{-i\omega_1 t} + \mathrm{E}_2 e^{-i\omega_2 t}$$

$$\mathbf{P} = \sum_i \mathbf{P}^{(i)} = \sum_i \chi^{(i)}\mathbf{E}^i$$

$$\boldsymbol{\omega_1, \omega_2}\colon \mathbf{P^{(1)}} = \chi^{(1)}\mathbf{E} = \chi^{(1)}\mathbf{E}_1 + \chi^{(1)}\mathbf{E}_2$$

$$\boldsymbol{\omega_2 - \omega_1, 2\omega_1, 2\omega_2}\colon \mathbf{P^{(2)}} = \chi^{(2)}\mathbf{E^2} = 2\chi^{(2)}\mathbf{E}_2\mathbf{E}_1^* + \chi^{(2)}\mathbf{E}_1^2 + 2\chi^{(2)}\mathbf{E}_1\mathbf{E}_2 + \chi^{(2)}\mathbf{E}_2^2$$

$$\boldsymbol{2\omega_1 - \omega_2, 2\omega_2 - \omega_1}\colon \mathbf{P^{(3)}} = \chi^{(3)}\mathbf{E^3} = 3\chi^{(3)}\mathbf{E}_1^2\mathbf{E}_2^* + 3\chi^{(3)}\mathbf{E}_2^2\mathbf{E}_1^* + \cdots$$

Notice the similarity between the expansion of the optical nonlinearity and the microwave nonlinearity (section 1.1.3.4.2 Distortion reduction techniques). The $\chi^{(1)}, \chi^{(2)}, \chi^{(3)}$ coefficients are determined by the material properties. If the material has inversion symmetry (is centrosymmetric) as

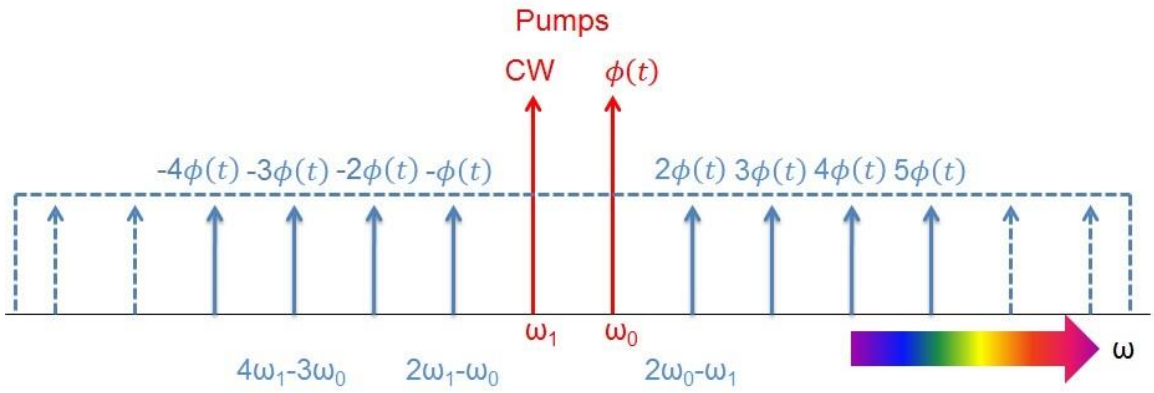

Figure 1.11 A cascaded four-wave mixing process between the signal and a CW pump laser is employed to produce idlers with integer multiples of the phase modulation of the original signal at frequencies which are integer multiples of $\Delta\omega_{comb} = \omega_1 - \omega_0$ away from the two pumps.

most materials do, then the $\chi^{(2)}$ term vanishes and $\chi^{(3)}$ becomes the first observable nonlinearity. FWM is one of the nonlinear processes that results from the $\chi^{(3)}$ nonlinearity. It is a process in which three lightwaves impinging on optical fiber produce a fourth lightwave whose frequency and phase are linear combinations of the original three. Energy and momentum are conserved among the four waves. Degenerate FWM occurs when not all three of the lightwaves are unique. Cascaded FWM is when the fourth wave produced continues propagating through the fiber and becomes one of the incident lightwaves in a subsequent FWM process, producing a fifth lightwave, and so on (see Fig. 1.11).

1.2.2 Stimulated Brillouin Scattering

Another class of nonlinear responses is inelastic, or nonparametric, meaning that energy is exchanged between the light and the medium. That is, the total light energy before and after entering the medium are unequal and the energy difference is absorbed or provided by the medium. SBS is one such nonlinear process. Originally observed by Ippen and Stolen in 1972 [50], SBS is a process by which incident photons of high intensity produce density and pressure variations in the lattice via electrostriction or expansion and are then scattered off by the resulting refractive index variations [51]. In standard optical fiber, the scattered photons are Stokes-shifted approximately 11 GHz below the incident frequency and the lattice absorbs the difference in energy between the incident and scattered photon in the form of acoustic vibrations known as phonons.

At low optical power and short link lengths, the effect of SBS is minor. However, as power increases, the proportion of incident power that is reflected increases. Beyond a certain threshold, almost all the incident power is reflected. This threshold optical power is determined by the properties of the fiber:

$$P_{SBS} = \frac{21A_{eff}}{g_B L_{eff}}$$

In standard single mode fiber, A_{eff} is 85 μm^2 and the nonlinear coefficient g_B

is $4x10^{-11}$ m/W, making the SBS threshold approximately:

$$P_{SBS} = \frac{42}{L_{eff}}$$

and since

$$L_{eff} = \frac{1 - e^{-\alpha L}}{\alpha}$$

as $L \to \infty$,

$$L_{eff} \cong \frac{1}{\alpha} \cong 21 \text{ km}$$

Therefore, $P_{SBS} = 2$ mW for link lengths ≥ 21 km [6].

In this thesis, SBS is a concern when trying to produce FWM by launching high power into highly nonlinear fiber (HNLF). Since the effective area of HNLF (11.7 μm^2) is smaller than single mode fiber and the nonlinear coefficient is also greater, the SBS threshold power is much lower and as a result, techniques for SBS mitigation must be explored. Several different techniques are mentioned in [6] including using alternating sections of fiber with different SBS frequencies, spans of fiber with SBS frequency distributions, fiber spans with nonuniform fiber dopants, fibers with unique refractive index profiles, polarization scrambling, broadening of input signal, suppressed-carrier modulation formats, temperature distribution, and strain distribution. We use a strain distribution to mitigate SBS in our architecture [52].

With this groundwork, we proceed in the remaining chapters to explain our link linearization idea, its architecture, and the experimental results.

2 Theory of Operation

In this chapter we explain the architecture and operation of the linearized phase-modulated link. To do this, we first explain the nonlinearities introduced by the conventional phase-modulated link, then we describe the optical nonlinearity we seek to introduce and how we produce it, and finally we show how together, with the appropriate choice of parameters, we can use them to cancel each other and make the system as a whole more linear.

2.1 Conventional ΦMID Link

In a ΦMID conventional link, the microwave signal modifies the refractive index of the lithium niobate within the electro-optic modulator via the Pockels effect, thereby modifying the phase of the propagating light. Following chapter 20 in [53]

$$\phi_{opt} = \frac{2\pi n(E) L}{\lambda_0}$$

$$n(E) = n - \frac{1}{2}\tau n^3 E$$

$$V_\pi = \frac{d}{L}\frac{\lambda_0}{\tau n^3}$$

$$\phi_{opt} = \phi_0 - \pi\frac{V}{V_\pi}$$

Let's say $V = V_0 \sin \omega_{\mu wave} t$, then the optical wave will be:

$$Ae^{i\omega_{opt}t+i\pi\frac{V_0}{V_\pi}\sin\omega_{\mu wave}t}$$

$$= Ae^{i\omega_{opt}t}\left(e^{i\pi\frac{V_0}{V_\pi}\sin\omega_{\mu wave}t}\right)$$

To expand the term within the parentheses, we use the Jacobi-Anger identity [54]:

$$e^{i\pi\frac{V_0}{V_\pi}\sin\omega_{\mu wave}t} = \sum_{n=-\infty}^{\infty} J_n\left(\pi\frac{V_0}{V_{pi}}\right)e^{in\omega_{\mu wave}t}$$

where J_n is the nth Bessel function of the first kind.

We can readily see that in the microwave domain we will have an infinite number of harmonics of the original microwave tone. However, if we were to place a photodetector immediately after the phase modulator (i.e. no a-MZI), we would see no microwave signal at all. The reason for this is in the optical domain each pair of sidebands equidistant from the optical carrier has a phase relationship such that when they cancel each other out when beat at the photodetector. When we use a device that has a non-uniform frequency response, we change the phase relationships such that not all the sidebands cancel. An a-MZI is one device that has such a response but it is not the only possible one that can be used. Indeed, there have recently been several experiments employing other demodulation techniques, such as using dispersive fiber [55].

In an a-MZI biased at quadrature and assuming small signals, we can calculate the response by performing a Taylor expansion (see blue curve in Fig. 2.1). We use the Taylor expansion for its simplicity in communicating

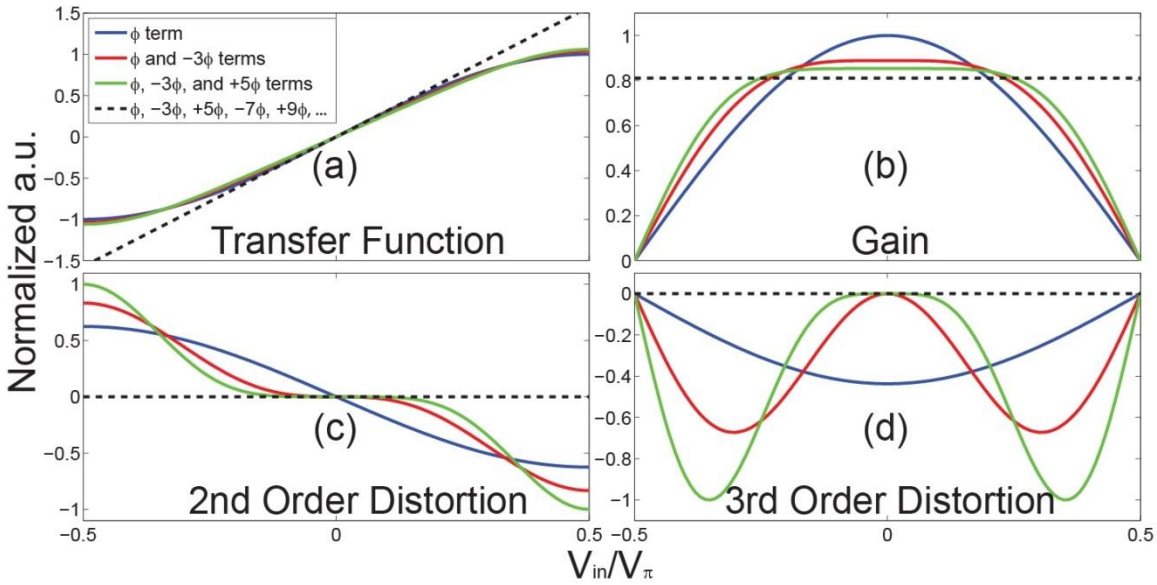

Figure 2.1 (a) The normalized transfer function with various Fourier terms (solid lines) and ideal (dotted); (b) 1st derivative of transfer function or normalized link gain; (c) 2nd derivative or second-order distortion; (d) 3rd derivative or third-order distortion.

the idea. If we were to use a Bessel function expansion instead, our coefficients (and the scaling factors given in section 2.2.2) would change but the numbers could be easily adjusted and the same techniques and analyses would apply. The Taylor expansion of a sine function about its inflection point is:

$$\sin\phi(t) = \phi(t) - \frac{\phi(t)^3}{3!} + \frac{\phi(t)^5}{5!} - \cdots$$

where ϕ(t) is the analog phase-encoded temporal signal. Notice that in addition to the desired linear term, there are higher odd order distortion products present. However, due to the quadrature bias, there are no even order distortion products present. In addition to the bias point, the frequency

response of the a-MZI also ensures that no even order products are present. Further, notice that the linear term has the highest coefficient and the coefficients decay rapidly as the order of the nonlinearity increases due to the factorial in the denominator. Finally, notice that if the magnitude of the signal (the phase) were to increase, the highest order nonlinearities would increase the fastest due to the magnitude of the exponent in the numerator. The magnitude of the higher order nonlinearities are so low to begin with, however, that to actually see them increase faster than the fundamental term, the power would have to be increased beyond the instrument noise floor, which is not always practical given the other device limitations in the system. This is confirmed by what we find in real systems.

2.2 Linearized ΦMID Link

Before delving into linearization, first consider two links: one with high CW laser power and a single tone excitation of low microwave power driving the phase modulator, the other with low CW laser power and a single tone excitation of high microwave power (see Fig. 2.2). Assume the a-MZIs have the same path length imbalance, τ, the same laser and microwave frequencies, and are both biased at quadrature. In both cases, the phase modulation produces sidebands spaced at integer multiples of $\omega_{\mu wave}$ on either side of the optical carrier that result in harmonics in the microwave

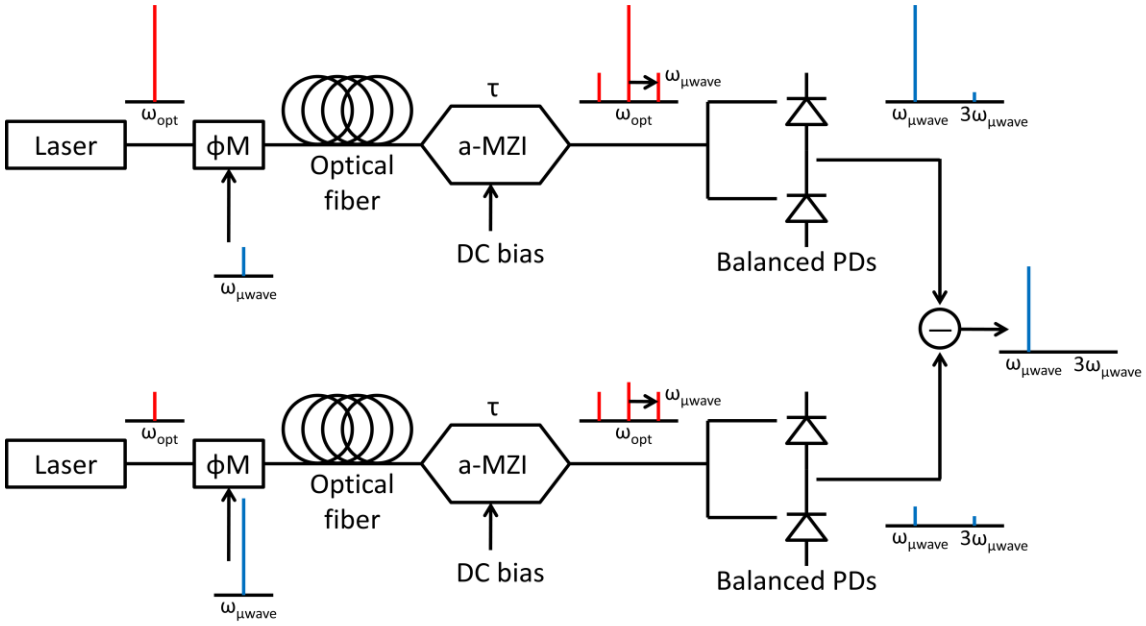

Figure 2.2 (upper) Conventional ΦMID link with high optical power (red) and low microwave power (blue); (lower) conventional ΦMID link with low optical power and high microwave power. Notice there is no $2\omega_{\mu wave}$ term and the $3\omega_{\mu wave}$ terms are equal. Together, after subtraction, the link is more linear. The fundamental is diminished and the $3\omega_{\mu wave}$ is eliminated.

domain. What differs between the two is the ratio of the powers of the distortion product to the fundamental tone. Because they are different, if we can tune the microwave and optical powers to equalize the powers in the distortion products and perform a subtraction, we can eliminate the distortion product in exchange for a slightly diminished fundamental tone. Thus, the system as a whole would be more linear. Since it is not possible to have two a-MZIs in which every distortion product (3rd order, 5th order, 7th

order, …) is equal but the fundamental tone is not, there will be higher order distortion products (5^{th} and beyond) still present in the system after the subtraction. We could add a third branch and re-tune the microwave and optical powers for all three such that when the outputs are combined both the third and fifth order distortion products are eliminated. In fact, we can continue this process indefinitely with an infinite number of a-MZIs to eliminate all distortion products. With a few adjustments, this is essentially the idea behind our linearization architecture.

One thing that is immediately noticeable when looking at Fig. 2.2 is

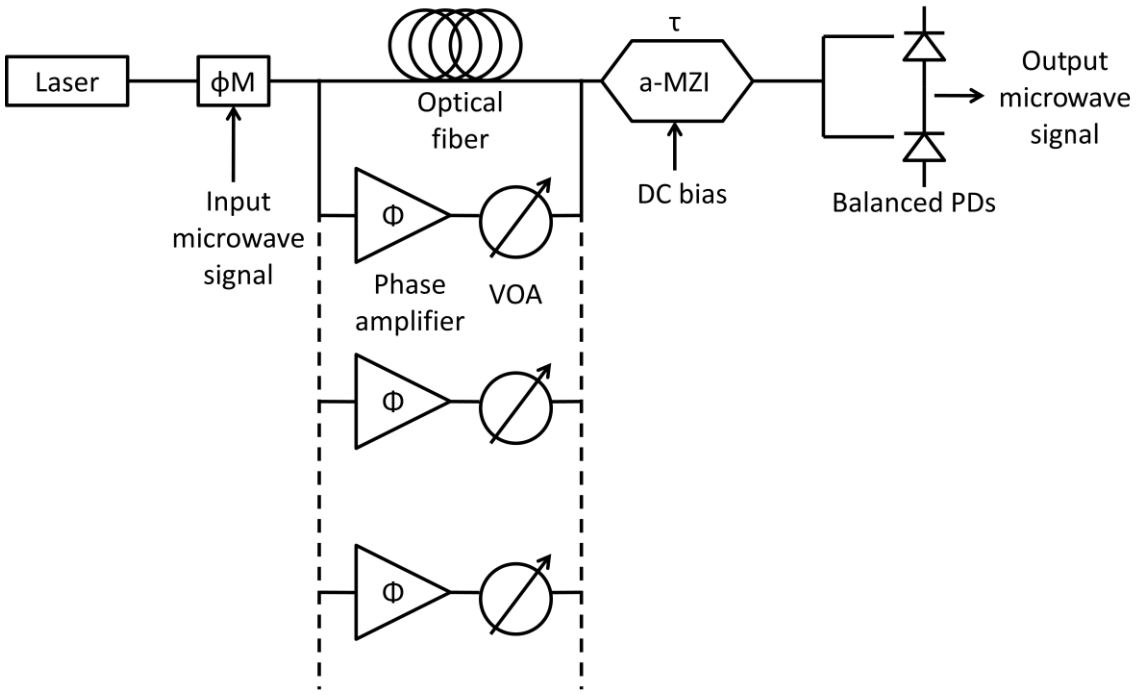

Figure 2.3 Linearized ΦMID link with each branch, consisting of a phase amplifier and variable optical attenuator (VOA), capable of eliminating one distortion product. Additional branches (dashed lines) can be added to eliminate more distortion products.

that the architectures of the two links are identical and only the input powers into the devices are different. This suggests that using splitters and combiners we may able to re-use the link components. Indeed, by using a phase amplifier in the linearization branch and appropriately choosing the splitting ratio and attenuation in the variable optical attenuator (VOA), we can replicate the effect of a different microwave to optical power ratio (see Fig. 2.3). By adding additional linearization branches we can eliminate higher order distortions.

In the following sections we go into detail about how we can use a nonlinear optical process and a flexible filter/attenuator to perform multiple orders of distortion elimination with a single linearization branch, then we explain the architecture of this system and how we assign and incorporate the scaling coefficients.

2.2.1 How it works

In the introduction we mentioned degenerate cascaded four-wave mixing as a nonlinear optical process in which the frequencies and phases of the generated lightwaves are linear combinations of the incident lightwaves. Here we will show how to exploit this. Consider two pumps incident on a spool of HNLF, a phase-modulated optical signal and an unmodulated continuous-wave laser (see Fig. 2.4 [56, 57]), which are separated by a

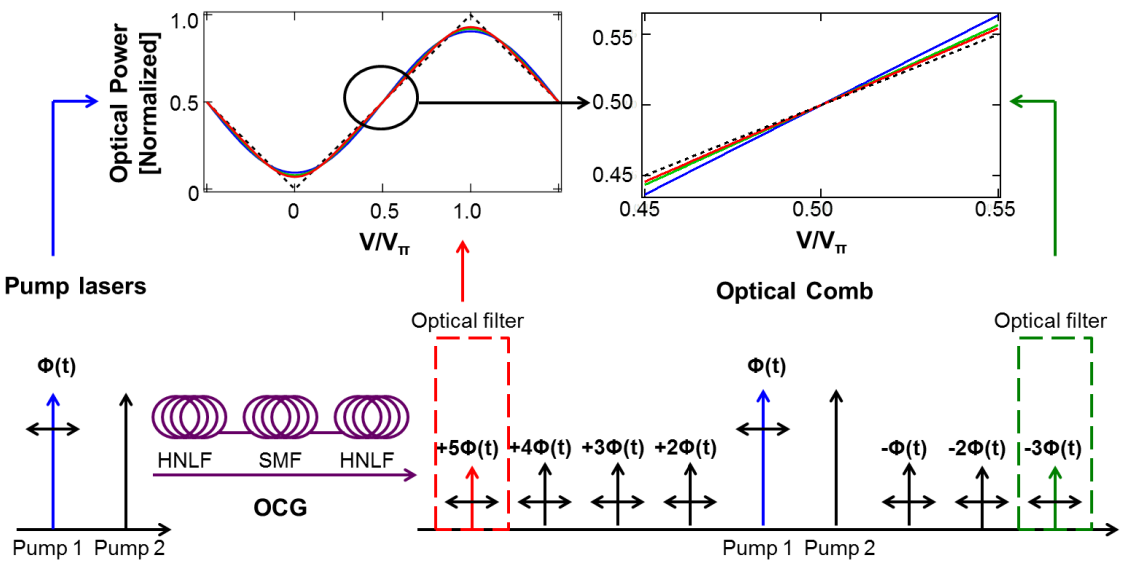

Figure 2.4 The lower figure shows the cascaded four-wave mixing process produces idlers that are filtered, scaled and combined to linearize the electro-optic transfer function. The upper plot shows the transfer function of just the conventional link (blue), the third-order distortion free link (green), the simultaneous third- and fifth-order distortion free link (red), and the ideal linear link (dashed black).

frequency, Δf_{comb}, much greater than the bandwidth of operation. Each of the optical frequencies should also fall within a small band of the peak of the a-MZI response (i.e. they should be close to an integer multiple + ½ times the a-MZI bandwidth, or $N + \frac{1}{2} = \tau \Delta f_{comb}$).

As the two lightwaves propagate down the fiber, they produce an optical comb, or an array of lightwaves at regular Δf_{comb} spacings around the pumps. While the efficiency of the FWM process is polarization dependent, by implementing a polarization diversity technique it is possible to eliminate this dependency with increased receiver complexity if necessary [58]. The

frequencies produced are $\pm(N * f_{pump1} - M * f_{pump2})$, where N and M are integers, and their phases are also $\pm(N * \Phi_{pump1} - M * \Phi_{pump2})$ respectively. Since the second pump is unmodulated, $\Phi_{pump2} = 0$, but we discuss this further in chapter five. Thus the phases of the lightwaves are $\pm N * \Phi_{pump1}$ and we have achieved our goal of phase amplification, with N being the gain factor.

To understand how we can eliminate distortion, let us re-examine the sinusoidal response of the a-MZI at quadrature, this time comparing it to the response of a phase amplified version of the signal:

$$\sin\phi(t) = \phi(t) - \frac{\phi(t)^3}{3!} + \frac{\phi(t)^5}{5!} - \cdots$$

$$\sin 3\phi(t) = 3\phi(t) - \frac{(3\phi(t))^3}{3!} + \frac{(3\phi(t))^5}{5!} - \cdots$$

Notice that while the linear term triples in the phase amplified version, the third-order distortion product increases by a factor of 27. Thus if we can scale the phase amplified version by 1/27 and subtract, we can eliminate the third-order distortion product at the cost of a slight reduction in link gain (see red curve in Fig. 2.1):

$$\sin\phi(t) - \frac{1}{27}\sin 3\phi(t) = \frac{8}{9}\phi(t) - \frac{1}{15}\phi(t)^5 + \cdots$$

We can perform such a scaling by using a filter centered at the comb line with the appropriate phase multiple, followed by a VOA to tune the optical power of that line to the desired value. The remaining fifth-order term is of higher

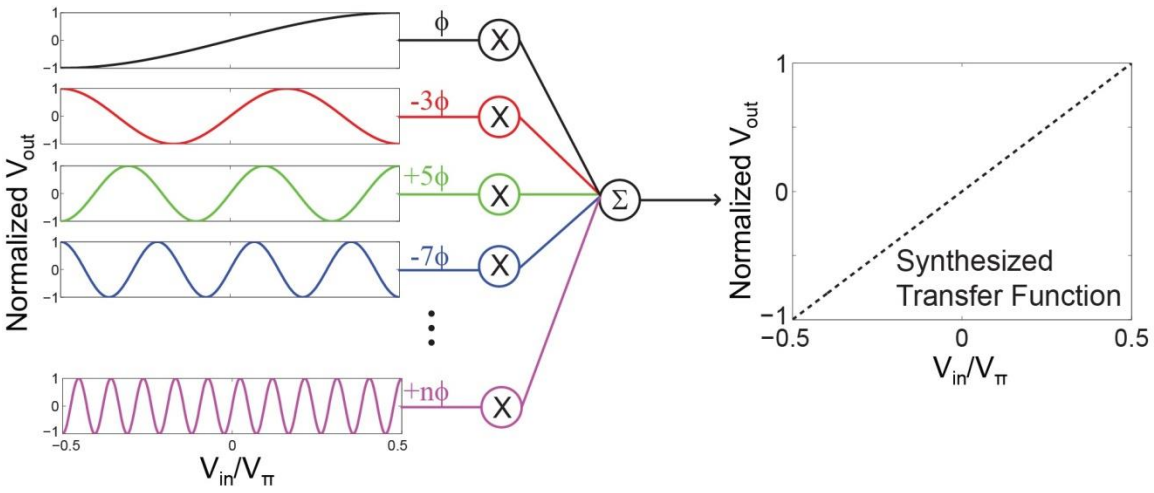

Figure 2.5 By appropriately choosing, scaling, and combining lightwaves with the correct phase multiples of the original signals, any transfer function can be synthesized.

magnitude than the original fifth-order distortion present in the conventional link. However, by adding more scaled lightwaves and following a similar process, it is possible to further eliminate higher-order distortion products, which also increases the quadrature bias tolerance of the interferometer (see green curve in Fig. 2.1). The scale coefficients of the added lightwaves are readily found using a matrix inversion as detailed in the next section. Furthermore, in the limit as the number of terms $m \to \infty$, the scale coefficients asymptotically approach those of the Fourier expansion of a triangle wave and the transfer function is perfectly linear (see Fig. 2.5). The scale factors can be applied in this case with a programmable spectral filter such as a Finisar Waveshaper. With this device, complex filter functions with different amounts of attenuation for each pass band can be applied through software.

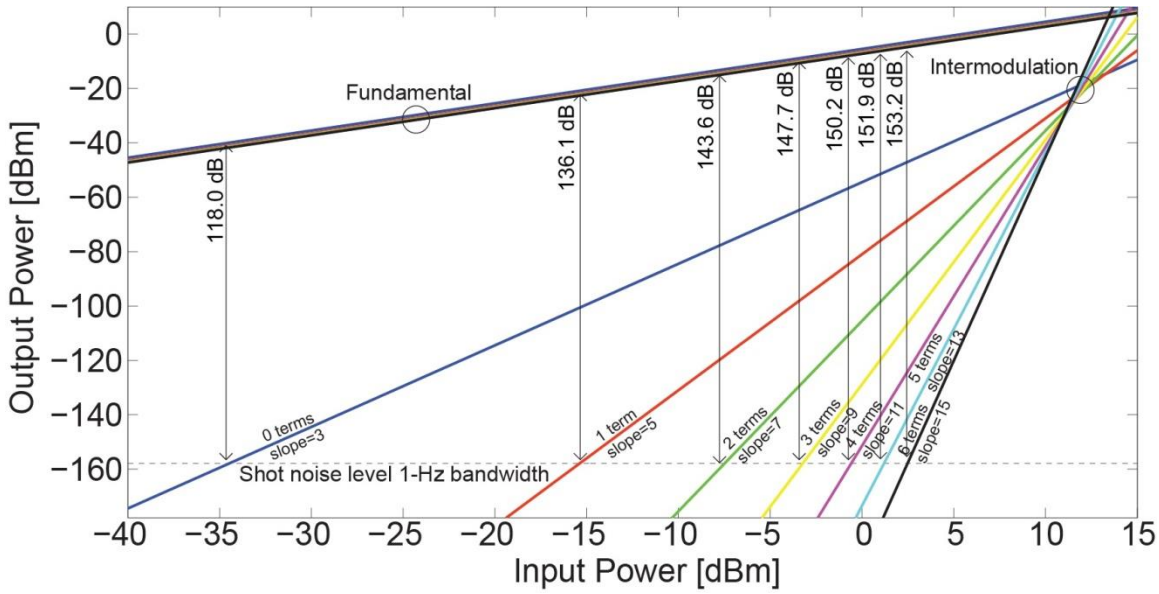

Figure 2.6 Theoretical SFDR performance calculated for the ΦMID link as an increasing number of linearization terms are added and assuming a modulator V_π of 5.9 V and 5-mA per photodetector with balanced detection

To investigate the impact of this linearization on the SFDR of the ΦMID link, we calculated the SFDR resulting from the fundamental tone and the intermodulation product generated by a two-tone test using the coefficients found by the method described above. To best compare with our experimental results, we use our experimental link parameters in this calculation. Namely, we assume a modulator V_π of 5.9 V and a photocurrent of 5 mA for each detector in balanced configuration. In Fig. 2.6 we plot the received fundamental and intermodulation power as a function of microwave power input to the link. Here for SFDR calculation we assume a shot noise limited link. For these link parameters Fig. 2.7 shows the SFDR at 1-Hz

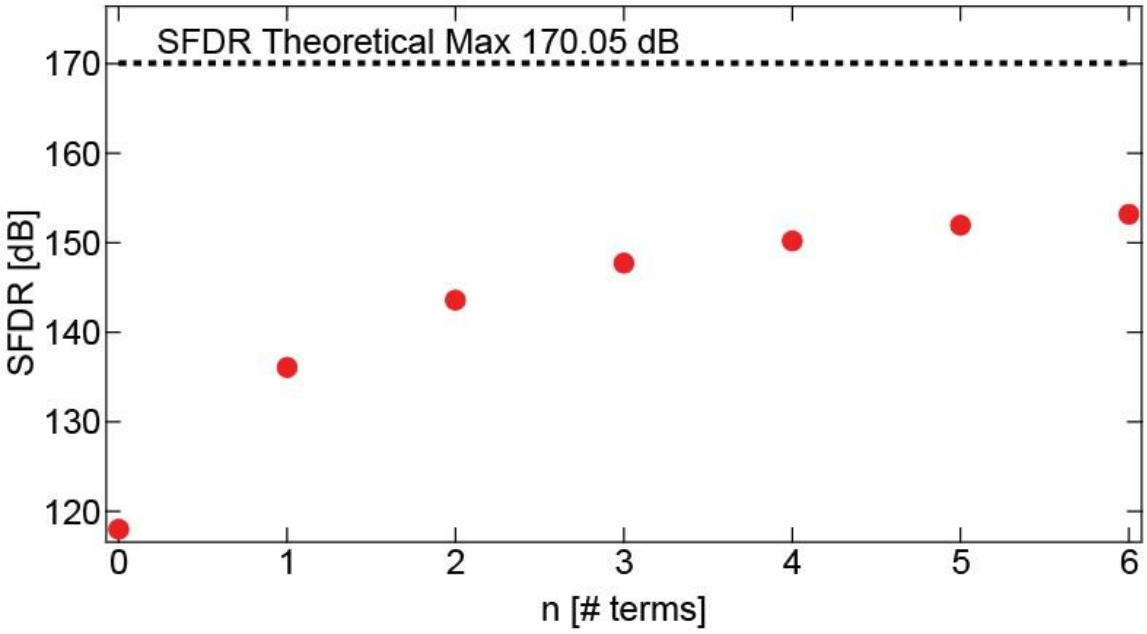

Figure 2.7 The calculated SFDR as an increasing number of linearization terms are added. The dashed line represents the SFDR for a perfectly linear link when the maximum peak to peak voltage equals the modulator V_π for reference.

bandwidth as a function of the number of linearization terms. The link SFDR also depends on signal bandwidth and we plot the SFDR versus bandwidth as a function of the number of linearization terms in Fig. 2.8. The advantages of this linearization approach are multifold. Firstly, additional lightwaves can be added with no increase in hardware complexity, so it is possible to linearize many orders of distortion in the link as demonstrated here. Secondly, as long as the filter is dynamically reconfigurable, distortion products can be added or removed at will (perhaps for testing) and the link can be continuously tuned or optimized. Thirdly, all-optical processing is inherently wide-bandwidth and will not limit the operating bandwidth of the

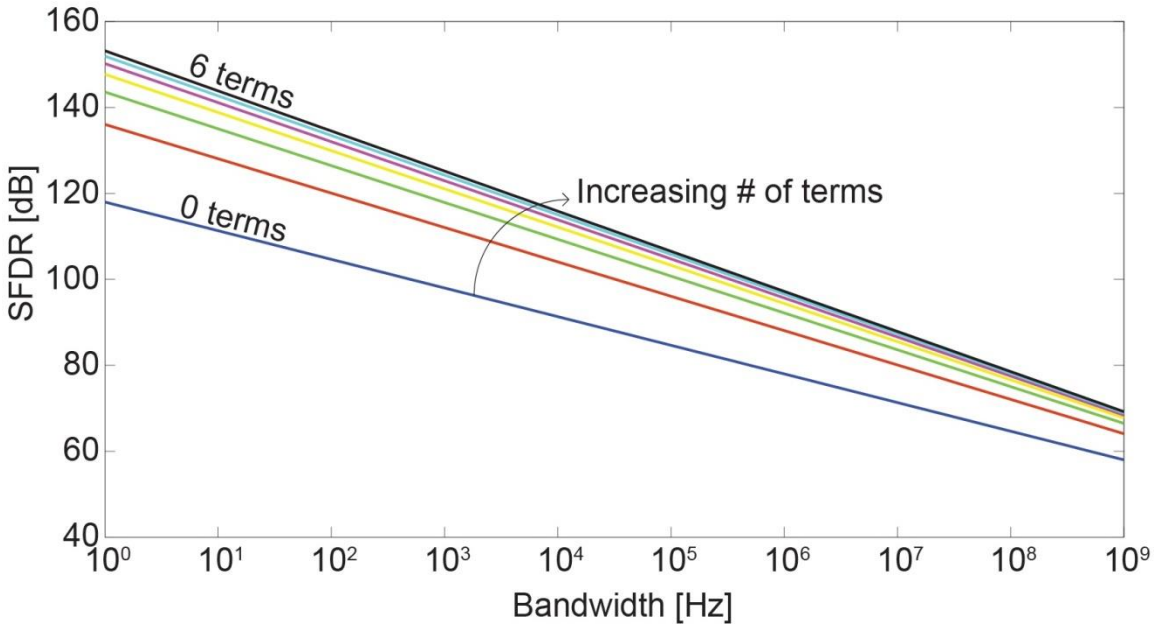

Figure 2.8 The calculated SFDR versus signal bandwidth for different numbers of linearization terms.

additional optical signal processing functionalities within the link. Lastly, because the linearization is accomplished completely optically, it is straightforward to incorporate into the link. Beyond linearization, for example, these Fourier components can also be scaled and combined to yield any custom-made transfer function through a Fourier synthesis approach. Such arbitrary transfer functions could potentially eliminate the need for electronic components before or after the link. For example, by introducing the inverse nonlinearity of a microwave component after the link on top of a linear transfer function, we could make the link act as a predistorter that would enhance the performance of the overall system.

2.2.2 Determination of Fourier Coefficients

Here we show how to derive the scaling factors for the Fourier coefficients of a linear transfer function, assuming quadrature bias and thus no even order distortion. Starting with two lightwaves $\phi(t)$ and $3\phi(t)$ and using the first two terms of the Taylor expansion, we can readily solve for the scaling factor required for the second lightwave to eliminate the third-order distortion and leave only the linear term:

$$\sin\phi(t) = \phi(t) - \frac{\phi(t)^3}{3!} + \cdots$$

$$a_1 \sin 3\phi(t) = a_1 3\phi(t) - \frac{a_1(3\phi(t))^3}{3!} + \cdots$$

$$\sin\phi(t) + a_1 \sin 3\phi(t) = (1 + 3a_1)\phi(t)$$

$$[3^3][a_1] = [-1]$$

$$[a_1] = \left[-\tfrac{1}{27}\right]$$

Now, if we add another lightwave, $5\phi(t)$ and find the first three terms of the Taylor series, we can eliminate both the third and fifth order distortions. To do this, we must find the scaling factors for both the $3\phi(t)$ lightwave (because the scaling factors change as we change the number of lightwaves) as well as $5\phi(t)$ lightwave. We can do this by performing the following matrix inversion:

$$\sin\phi(t) = \phi(t) - \frac{\phi(t)^3}{3!} + \frac{\phi(t)^5}{5!} - \cdots$$

$$+ a_1 \sin 3\phi(t) = a_1 3\phi(t) - \frac{a_1(3\phi(t))^3}{3!} + \frac{a_1(3\phi(t))^5}{5!} - \cdots$$

$$+ a_2 \sin 5\phi(t) = a_2 5\phi(t) - \frac{a_2(5\phi(t))^3}{3!} + \frac{a_2(5\phi(t))^5}{5!} - \cdots$$

$$\sin\phi(t) + a_1 \sin 3\phi(t) + a_2 \sin 5\phi(t) = (1 + 3a_1 + 5a_2)\phi(t)$$

$$\begin{bmatrix} 3^3 & 5^3 \\ 3^5 & 5^5 \end{bmatrix} \begin{bmatrix} a_1 \\ a_2 \end{bmatrix} = \begin{bmatrix} -1 \\ -1 \end{bmatrix}$$

$$\begin{bmatrix} a_1 \\ a_2 \end{bmatrix} = \begin{bmatrix} -\frac{1}{18} \\ \frac{1}{250} \end{bmatrix}$$

In general, we can remove the first $(2m+1)$ distortions by adding m lightwaves, as follows:

$$\sin\phi(t) = \phi(t) - \frac{\phi(t)^3}{3!} + \frac{\phi(t)^5}{5!} + \cdots + \frac{(-1)^m \phi(t)^{2m+1}}{(2m+1)!} + \cdots$$

$$+ a_1 \sin 3\phi(t) = a_1 3\phi(t) - \frac{a_1\left(3\phi(t)\right)^3}{3!} + \frac{a_1\left(3\phi(t)\right)^5}{5!} + \cdots + \frac{a_1(-1)^m(3\phi(t))^{2m+1}}{(2m+1)!}$$

$$+ \cdots$$

$$+ a_2 \sin 5\phi(t) = a_2 5\phi(t) - \frac{a_2(5\phi(t))^3}{3!} + \frac{a_2(5\phi(t))^5}{5!} + \cdots + \frac{a_2(-1)^m(5\phi(t))^{2m+1}}{(2m+1)!}$$

$$+ \cdots$$

$$+ a_m \sin(2m+1)\phi(t)$$

$$= a_m(2m+1)\phi(t) - \frac{a_m\big((2m+1)\phi(t)\big)^3}{3!} + \frac{a_m((2m+1)\phi(t))^5}{5!} + \cdots$$

$$+ \frac{a_m(-1)^m((2m+1)\phi(t))^{2m+1}}{(2m+1)!} + \cdots$$

$$\sin\phi(t) + a_1 \sin 3\phi(t) + a_2 \sin 5\phi(t) + \cdots + a_m \sin(2m+1)\phi(t) =$$

$$(1 + 3a_1 + 5a_2 + \cdots (2m+1)a_m)\phi(t)$$

$$\begin{bmatrix} 3^3 & \cdots & (2m+1)^3 \\ \vdots & \ddots & \vdots \\ 3^{2m-1} & \cdots & (2m+1)^{2m+1} \end{bmatrix} \begin{bmatrix} a_1 \\ \vdots \\ a_m \end{bmatrix} = \begin{bmatrix} -1 \\ \vdots \\ -1 \end{bmatrix}$$

$$\begin{bmatrix} a_1 \\ \vdots \\ a_m \end{bmatrix} = \begin{bmatrix} 3^3 & \cdots & (2m+1)^3 \\ \vdots & \ddots & \vdots \\ 3^{2m+1} & \cdots & (2m+1)^{2m+1} \end{bmatrix}^{-1} \begin{bmatrix} -1 \\ \vdots \\ -1 \end{bmatrix}$$

While the determination of the coefficients is necessary to understand the experimental setups given in the subsequent chapters, the observant reader will notice that the choice of lightwaves with odd integer multiples of the phase is not necessary. To show this, we can repeat our above analysis with even integer phase multiples and a mix of even and odd phase multiples, described with the b and c coeffecients, respectively.

$$\sin\phi(t) = \phi(t) - \frac{\phi(t)^3}{3!} + \cdots$$

$$b_1 \sin 2\phi(t) = b_1 2\phi(t) - \frac{b_1(2\phi(t))^3}{3!} + \cdots$$

$$\sin \phi(t) + b_1 \sin 2\phi(t) = (1 + 2b_1)\phi(t)$$

$$[2^3][b_1] = [-1]$$

$$[b_1] = \left[-\tfrac{1}{8}\right]$$

As we did before, if we add another lightwave, $4\phi(t)$ and find the first three terms of the Taylor series, we can eliminate both the third and fifth order distortions. To do this, we must find the scaling factors for both the $2\phi(t)$ lightwave as well as $4\phi(t)$ lightwave as follows:

$$\sin \phi(t) = \phi(t) - \frac{\phi(t)^3}{3!} + \frac{\phi(t)^5}{5!} - \cdots$$

$$+ b_1 \sin 2\phi(t) = b_1 2\phi(t) - \frac{b_1(2\phi(t))^3}{3!} + \frac{b_1(2\phi(t))^5}{5!} - \cdots$$

$$+ b_2 \sin 4\phi(t) = b_2 4\phi(t) - \frac{b_2(4\phi(t))^3}{3!} + \frac{b_2(4\phi(t))^5}{5!} - \cdots$$

$$\sin \phi(t) + b_1 \sin 2\phi(t) + b_2 \sin 4\phi(t) = (1 + 2b_1 + 4b_2)\phi(t)$$

$$\begin{bmatrix} 2^3 & 4^3 \\ 2^5 & 4^5 \end{bmatrix} \begin{bmatrix} b_1 \\ b_2 \end{bmatrix} = \begin{bmatrix} -1 \\ -1 \end{bmatrix}$$

$$\begin{bmatrix} b_1 \\ b_2 \end{bmatrix} = \begin{bmatrix} -\frac{5}{32} \\ \frac{1}{256} \end{bmatrix}$$

In general, we can remove the first $(2m+1)$ distortions by adding m lightwaves, with the following coefficients:

$$\begin{bmatrix} b_1 \\ \vdots \\ b_m \end{bmatrix} = \begin{bmatrix} 2^3 & \cdots & (2m)^3 \\ \vdots & \ddots & \vdots \\ 2^{2m+1} & \cdots & (2m)^{2m+1} \end{bmatrix}^{-1} \begin{bmatrix} -1 \\ \vdots \\ -1 \end{bmatrix}$$

The first c coefficient is the same as the first b coefficient:

$$\sin\phi(t) = \phi(t) - \frac{\phi(t)^3}{3!} + \cdots$$

$$c_1 \sin 2\phi(t) = c_1 2\phi(t) - \frac{c_1(2\phi(t))^3}{3!} + \cdots$$

$$\sin\phi(t) + c_1 \sin 2\phi(t) = (1 + 2c_1)\phi(t)$$

$$[2^3][c_1] = [-1]$$

$$[c_1] = \left[-\frac{1}{8}\right]$$

The difference between the b and c coefficients arises with the addition of the next lightwave, $3\phi(t)$:

$$\sin\phi(t) = \phi(t) - \frac{\phi(t)^3}{3!} + \frac{\phi(t)^5}{5!} - \cdots$$

$$+c_1 \sin 2\phi(t) = b_1 2\phi(t) - \frac{c_1(2\phi(t))^3}{3!} + \frac{c_1(2\phi(t))^5}{5!} - \cdots$$

$$+c_2 \sin 3\phi(t) = c_2 3\phi(t) - \frac{c_2(3\phi(t))^3}{3!} + \frac{c_2(3\phi(t))^5}{5!} - \cdots$$

$$\sin\phi(t) + c_1 \sin 2\phi(t) + c_2 \sin 4\phi(t) = (1 + 2c_1 + 4c_2)\phi(t)$$

$$\begin{bmatrix} 2^3 & 3^3 \\ 2^5 & 3^5 \end{bmatrix} \begin{bmatrix} c_1 \\ c_2 \end{bmatrix} = \begin{bmatrix} -1 \\ -1 \end{bmatrix}$$

$$\begin{bmatrix} c_1 \\ c_2 \end{bmatrix} = \begin{bmatrix} -\frac{1}{5} \\ \frac{1}{45} \end{bmatrix}$$

In general, we can remove the first $(2m+1)$ distortions by adding m lightwaves, with the following coefficients:

$$\begin{bmatrix} c_1 \\ \vdots \\ c_m \end{bmatrix} = \begin{bmatrix} 2^3 & \cdots & (m-1)^3 \\ \vdots & \ddots & \vdots \\ 2^{2m+1} & \cdots & (m-1)^{2m+1} \end{bmatrix}^{-1} \begin{bmatrix} -1 \\ \vdots \\ -1 \end{bmatrix}$$

Notice that all the coefficients, $a, b,$ and c have the form:

$$\begin{bmatrix} \alpha_1^3 & \cdots & \alpha_m^3 \\ \vdots & \ddots & \vdots \\ \alpha_1^{2m+1} & \cdots & \alpha_m^{2m+1} \end{bmatrix} \begin{bmatrix} x_1 \\ \vdots \\ x_m \end{bmatrix} = \begin{bmatrix} -1 \\ \vdots \\ -1 \end{bmatrix}$$

We can rewrite the coefficient matrix as:

$$\begin{bmatrix} 1 & \cdots & 1 \\ \vdots & \ddots & \vdots \\ \alpha_1^{2m-2} & \cdots & \alpha_m^{2m-2} \end{bmatrix} \begin{bmatrix} \alpha_1^3 & \cdots & 0 \\ \vdots & \ddots & \vdots \\ 0 & \cdots & \alpha_m^3 \end{bmatrix} \begin{bmatrix} x_1 \\ \vdots \\ x_m \end{bmatrix} = \begin{bmatrix} -1 \\ \vdots \\ -1 \end{bmatrix}$$

The first matrix (A) is the transpose of the Vandermonde matrix and the second matrix (B) is a diagonal matrix whose elements are the first row of the original coefficient matrix. The coefficients $x_1, x_2, x_3, \ldots x_m$ can be found using the following facts,

$$(AB)^{-1} = B^{-1}A^{-1}$$

$$A^{-1} = \frac{1}{\det(A)} adj(A)$$

$$B^{-1} = \frac{1}{\det(B)} adj(B)$$

$$\det(AB) = \det(A)\det(B)$$

$$\det(A) = \det(A^T) = \prod_{1 \le i < j \le m} (\alpha_j - \alpha_i)$$

$$\det(B) = \alpha_1^3 \alpha_2^3 \ldots \alpha_1^3$$

where adj(A) denotes the adjugate matrix of A. This is useful especially in the cases where inverting the coefficient matrix of size $m \geq 10$ with geometrically progressing coefficients becomes intractable to solve for by standard computational software such as Matlab.

Regardless of which set of coefficients are used, in the limit as $m \to \infty$, all sets converge to the Fourier series for a triangle wave:

$$\frac{8}{\pi^2} \sum_{m=0}^{\infty} (-1)^m \frac{\sin[(2m+1)\phi(t)]}{(2m+1)^2}$$

Since any set of phase multiples can be used to perform the linearization, it is natural to ask which integer multiples of the phase to use: $a, b, c,$ or some other set. The answer depends on the experimental setup. Notice that the magnitude of the a coefficients are the lowest of the three given. Experimentally this means that the requirement for the magnitude of the $3\phi(t)$ lightwave coming from the lower linearization branch relative to the fundamental $\phi(t)$ lightwave coming from the upper conventional branch can be more easily met (via attenuation in the Waveshaper) than the requirement for the b or c coefficients for the $2\phi(t)$ lightwave, which would require additional optical amplification to achieve its required magnitude. Notice also that using higher-order coefficients has lower impact on the reduction in the fundamental tone. That is, with the a coefficients, the gain reduces by 0.16 or 0.25 dB with one or two coefficients, respectively. With the b coefficients, the gain reduces by 0.6 or 0.7, and with the c coefficients, the gain reduces by 0.6 or 1.0 dB. Finally, the remaining distortions after linearization are lower in magnitude with the a coefficients than with the b or c coefficients. All of these observations point to using the highest magnitude set of phase multiples. The obstacle to using a very high magnitude set of coefficients is the magnitude and optical bandwidth of the lightwaves at the edges of the gain-bandwidth curve of the FWM process, the bandwidth of the Waveshaper, and the ability to measure, and therefore eliminate, higher order distortion terms.

3 All-Optical Link Linearization (3rd Order)

3.1 Introduction

In this chapter, we present our novel method for distortion elimination in phase-modulated analog optical links. A small part of the phase modulated signal seeds a four-wave mixing comb source, which generates lightwaves with integer multiples of the phase modulation of the original signal. These lightwaves are scaled and re-combined with the original phase-modulated signal to cancel the distortion generated in the interferometric phase-to-amplitude conversion process. Experimentally, we demonstrate full cancelation of the third-order distortion of the receiver and achieve a 19-dB improvement in the link's SFDR at a 1-Hz bandwidth. This approach is readily extendable to eliminate all relevant higher-order distortion products or synthesize arbitrary phase-to-amplitude transfer functions.

3.2 Experiment

To experimentally investigate the linearization performance of this approach we construct a conventional ΦMID link and a linearized ΦMID link as depicted in Figs. 3.1 and 3.2. The conventional ΦMID link consists of a 20-mW laser operated at 1558.98 nm and a 20-GHz electro-optic phase

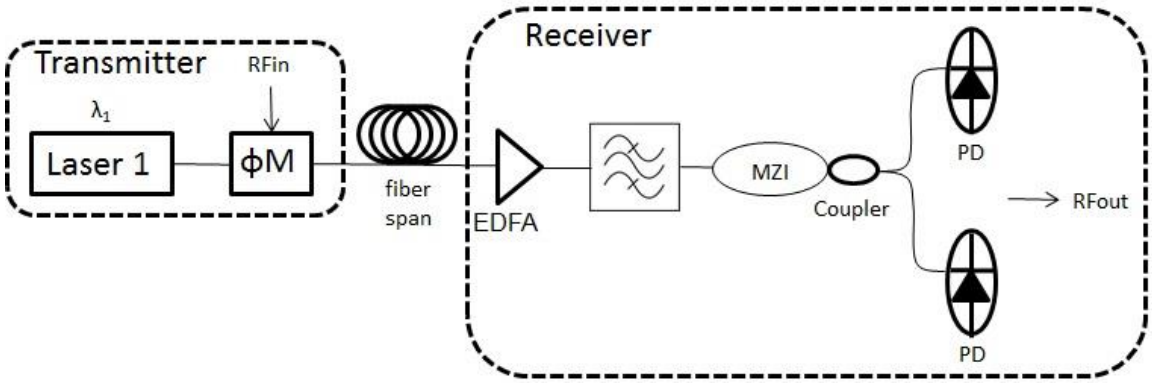

Figure 3.1 Experimental block diagram of conventional phase-modulated analog optical link. ΦM: phase modulator, MZI: asymmetric Mach-Zehnder interferometer, PD: photodetector.

modulator at the transmit end. At the receive end, we have an EDFA that receives about 10 mW and outputs 85 mW. A bandpass filter aligned with our laser wavelength removes the out of band amplified spontaneous emission noise from the signal. Finally, the phase modulated signal is detected using an asymmetric Mach-Zehnder interferometer (a-MZI), and a Discovery Semiconductors DSC740 balanced photodetector with 0.62 A/W responsivity and 26 GHz bandwidth (see Fig. 3.1). In the linearized ΦMID link, we use the same components, wavelengths, and power levels as in the conventional link, but we add several more components. After amplifying the phase-modulated signal, we tap off 10% and combine it with another CW laser at 1554.79 nm and 17 mW to seed the cascaded FWM comb generation process. This comb source consists of two cascaded spools of highly nonlinear fiber (HNLF), the first of which is 88-m long and is staircase-tensioned in ten

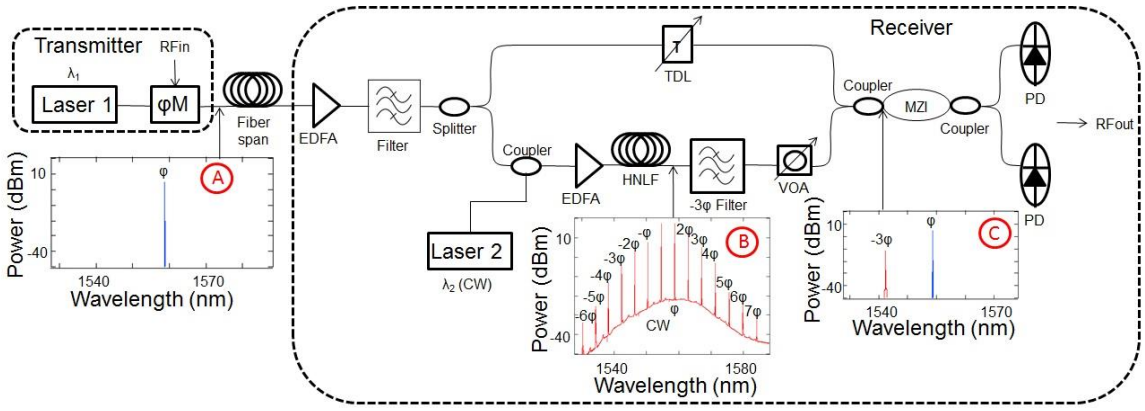

Figure 3.2 Experimental block diagram of the linearized link. EDFA: Erbium doped fiber amplifier, HNLF: highly nonlinear optical fiber, TDL: tunable delay line, -3ϕ filter: optical bandpass filter, VOA: variable optical attenuator, MZI: asymmetric Mach-Zehnder interferometer, PD: photodetector. Optical spectra at various points in the block diagram. A: Phase-modulated signal; B: Optical comb source output; C: Combined phase-modulated signal with -3ϕ component filtered from comb line.

steps from low to high tension to suppress Brillouin scattering, and the second of which is 100 m long and has uniform low tension [57]. We operate the EDFA prior to the comb generation at 2 W. After comb generation we isolate the -3$\phi(t)$ comb line by using an optical bandpass filter at 1542.94 nm. We introduce the scaling factor by attenuating the -3$\phi(t)$ signal with the variable optical attenuator (VOA) such that the intermodulation product is minimized. Our experimentally measured scale factor is about 1/24. Note the slight deviation from the theoretical value of 1/27 most likely results from compensation for additional sources of distortion in the link (e.g. the photodetector). Finally we combine this lightwave with the original signal

using a WDM filter and use the a-MZI and balanced photodetector to receive the combined signal (see Fig. 3.2).

For both links, we use a 100-ps path length difference in the a-MZI, which produces periodic dips spaced 10 GHz apart in the frequency response. Here we choose our center frequency to be the first peak near 5 GHz and our bandwidth is expected to be about 8 GHz based on Fig. 6 of [9]. The peak gain of the link is determined primarily by the V_π of the phase modulator and the current generated at the photodetector. For both links, we use the same 5.9-V V_π phase modulator and operate with 5-mA on each photodetector in the balanced receiver. We achieve a peak gain of -10.56 dB at 5 GHz in the linearized link and observe a small 1-dB reduction in the linearized link gain over the conventional link gain, as expected. We use a tunable delay line in the upper branch of the linearized ΦMID link in order to accurately path match it with the lower branch. With matched path lengths in the two branches the link bandwidth is unaffected by the linearization approach.

The noise figure of a phase-modulated link with balanced detection is primarily impacted by thermal noise in the detector, shot noise, and laser phase noise since laser relative intensity noise (RIN) is canceled through balanced detection [9]. We experimentally measure the noise figure of our link to be 39 dB for both the conventional as well as the linearized link. Thus the linearization approach adds negligible noise to the link. This is expected since the $\phi(t)$ lightwave represents the majority of the received power (upper

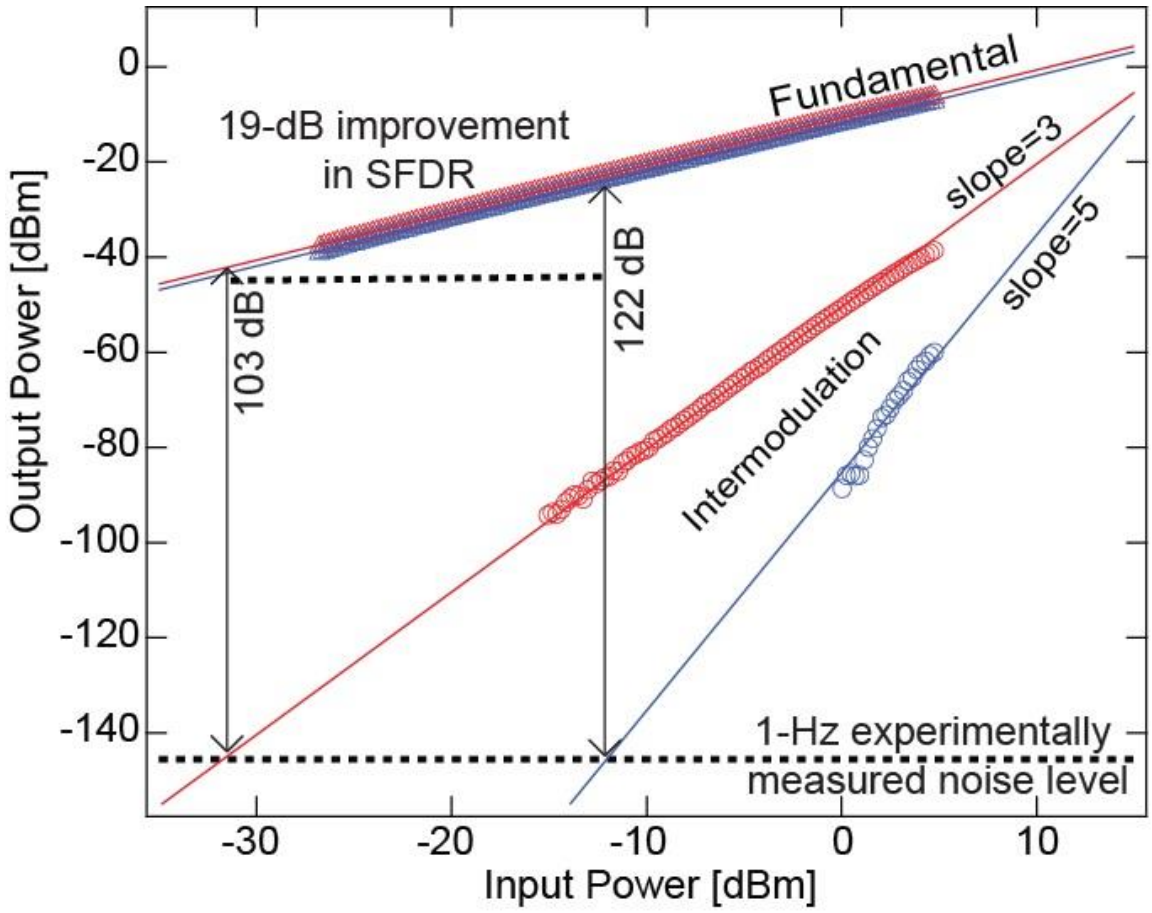

Figure 3.3 SFDR two-tone test (fundamental tones: 5.35 and 5.45 GHz, spurious tone: 5.25 and 5.55 GHz) comparison between conventional (red) and linearized (blue) phase-modulated analog optical link.

path in Fig. 3.2) and is not involved in the cascaded FWM interaction. In comparison, the -3$\phi(t)$ comb line represents only 1/24 of the received power relative to the $\phi(t)$ lightwave and thus any increase in the phase noise on the -3$\phi(t)$ line minimally impacts the noise figure of the link. Although balanced detection cancels the contribution of RIN to the link noise, the link is sensitive to the phase noise of the laser used. In our setup we use two New

Focus 6700 series External Cavity Tunable Diode Lasers with < 200 kHz linewidth. However, diode lasers exhibit relatively large phase noise in the GHz range thus we expect to be able to reduce the noise figure to near the shot noise limited level of 22.5 dB in future work by incorporating fiber lasers into the architecture [9].

We measure the SFDR using a two-tone test in which two microwave tones, one at 5.35 GHz the other at 5.45 GHz, are combined and applied to the input of the phase modulator. For sufficiently high microwave drive powers, spurious intermodulation tones at 5.25 GHz and 5.55 GHz are produced. By sweeping the powers of the input tones, we can determine the link SFDR. Fig. 3.3 shows the experimentally measured fundamental power and intermodulation power as a function of input power for both the conventional link and the linearized link. For the conventional link we obtain an SFDR of 103 dB based on our experimentally measured intermodulation characterization and experimentally measured noise level. With linearization we measure an SFDR of 122 dB, which represents a 19-dB improvement in SFDR for a 1-Hz noise bandwidth. Furthermore, we find that the intermodulation power now scales with the input power to the fifth indicating that the impact of third-order distortion is minimized over the measured power range. The slight increase in slope of the intermodulation power at the lower power levels is due to interference between residual third-order and fifth-order intermodulation products. This interference can be fully

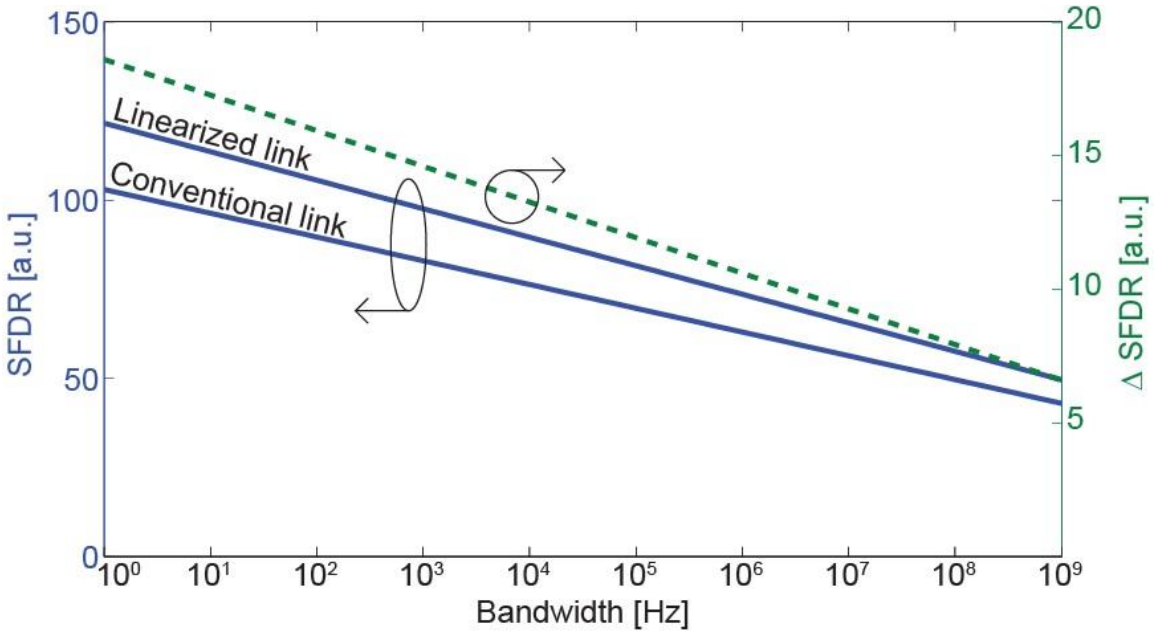

Figure 3.4 Experimental SFDR versus signal bandwidth for the experimentally characterized conventional link and linearized link. The SFDR improvement is also plotted (dashed line).

lightwave. Due to the change in slope of the intermodulation power from 3 to 5, the SFDR improvement over the conventional link depends on the signal bandwidth. Fig. 3.4 shows the link SFDR and SFDR improvement as a function of signal bandwidth based on the experimental characterizations.

3.3 Summary and Conclusion

We have demonstrated a novel receiver-based method for linearizing phase-modulated analog optical links. In this method, we tap off a small part of the modulated signal and use it along with an additional CW laser to seed

a cascaded FWM comb source. This source provides lightwaves with integer multiples of the original signal's phase modulation, which can be scaled and combined with the original signal to linearize the link using a Fourier approach. Experimentally we demonstrate full cancelation of third-order distortion and achieve a 19-dB improvement in link SFDR for a 1-Hz bandwidth. Furthermore, with this method, there is a straightforward path to eliminating higher order distortions as well as generating arbitrary link transfer functions.

4 All-Optical Link Linearization (3rd and 5th Orders)

4.1 Introduction

In this chapter, we experimentally demonstrate an all-optical architecture for linearization of a phase-modulated interferometrically-detected microwave photonic link. We couple off a small part of the phase-modulated signal and combine it with a pump lightwave to produce a comb of idlers in a cascaded four-wave mixing process. The phase-matching requirement of the cascaded process ensures that integer multiples of the original signal's temporal phase modulate each of the idlers. We accomplish the linearization by filtering, scaling, and re-combining a subset of the idlers. To the best of our knowledge, this is the first demonstration of a simultaneous third-order, fifth-order, and all even-order distortion free link in either intensity or phase modulated architectures. We experimentally measure a 108.8-dB SFDR for the conventional link, 116.1 dB for the third-order distortion-free link, and 116.9 dB for the third-order and fifth-order distortion-free link, each in a 1-Hz bandwidth. We show that the experimentally measured SFDR improvement is primarily limited by increased phase noise on the correction lightwaves. Specifically, we measure a 24.2-dB noise figure for the conventional link, 38.7 dB for the third-order distortion-free link, and 45 dB for the third-order and fifth-order distortion-free link. We discuss the source of this added noise and methods for

mitigation in future work, which could lead to a 134.8-dB SFDR in a 1-Hz bandwidth for a shot noise limited link with ~1 mA per photodiode.

4.2 Experiment

The experimental investigation presented here has three parts. In the first part, the conventional (unlinearized) ΦMID link is constructed and tested. For the second and third parts, the receiver portion is modified to introduce a branch where the optical nonlinearity is created. In the second part, only the third-order distortion product is eliminated and in the third part, both the third-order and fifth-order distortion products are simultaneously eliminated. For each of the three link realizations, the links are characterized with the four performance metrics: gain, bandwidth, noise figure, and SFDR. Aside from bandwidth, all the performance metrics are impacted to varying degrees. Specifically, gain is degraded by approximately 0.4 dB for each of the two eliminated distortion products and despite noise figure degradation with each additional term, SFDR is improved.

Gain is measured via an S21 measurement from 300 KHz to 20 GHz with a calibrated electronic network analyzer (ENA). Noise power is measured with a 50-Ohm termination at the input port of the phase modulator and an RF amplifier at the output to raise the link noise above the electronic spectrum analyzer noise floor. This data combined with the gain data allows us to calculate the noise figure for each of the three link

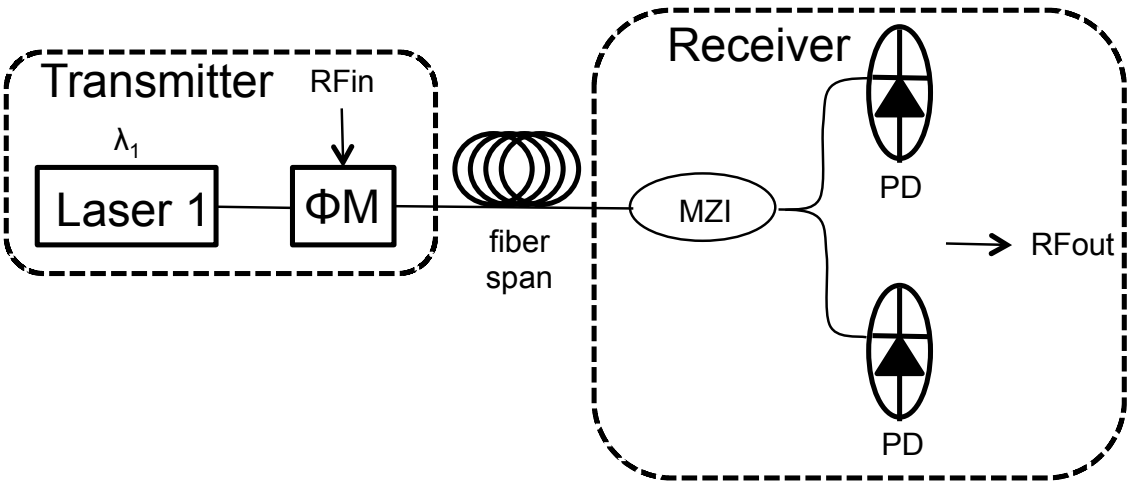

Figure 4.1 Experimental block diagram of conventional phase-modulated interferometrically detected (ΦMID) analog optical link. ΦM: phase modulator, MZI: asymmetric Mach-Zehnder interferometer, PD: photodetector.

realizations. To measure dynamic range, we perform a two-tone test, choosing the two tones close to the first peak of the a-MZI response. The first tone is injected by the ENA at 1.275 GHz and swept from –15 to 10 dBm. The second tone is injected by a signal generator at a constant power of 5 dBm. Both tones are sent through a low-pass filter to prevent any possible distortion terms generated by the test equipment from entering and skewing the distortion measurements of the link. These tones are combined and injected into the phase modulator input port. The second-order distortion products are minimized at 11 MHz and 2.561 GHz and the intermodulation distortion products are present at 1.264 GHz and 1.297 GHz. The retrieved data is mathematically corrected to reflect the fact that only one of the tones is swept in power.

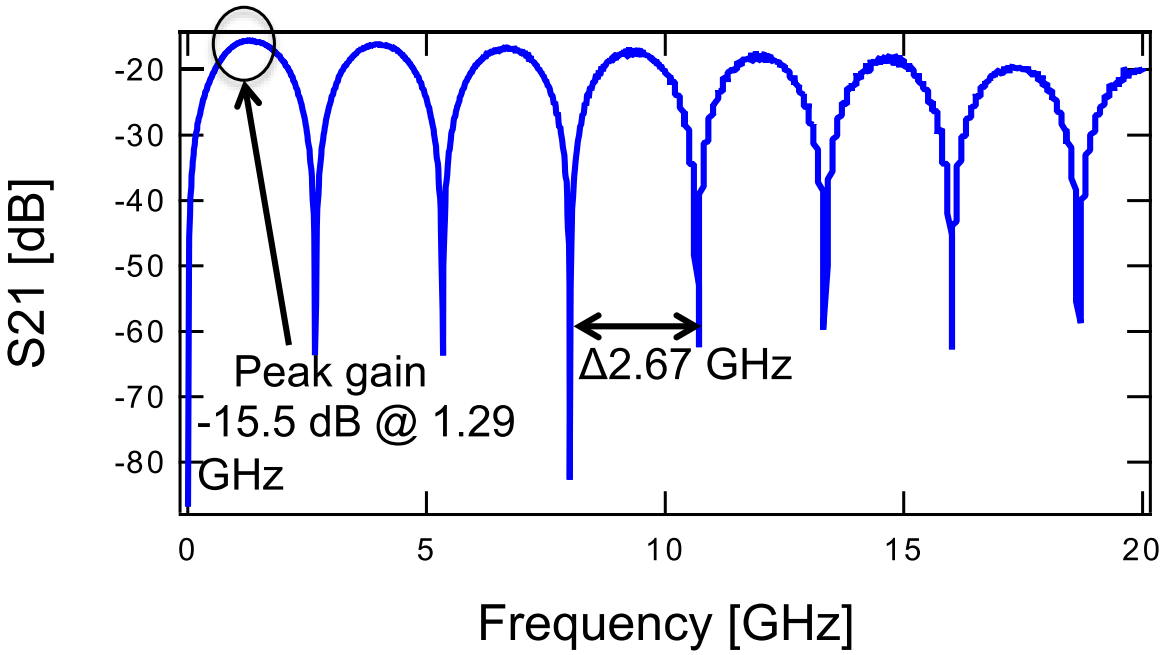

Figure 4.2 Experimental gain of the conventional ΦMID link. Note that we perform measurements at the first peak gain of about -15.5 dB around 1.29 GHz with 1.08 mA photocurrent. The 375-ps path length difference in the a-MZI produces periodic dips every 2.67 GHz.

4.2.1 Conventional Unlinearized Link

As shown in Fig. 4.1, the conventional link consists of a 50 mW low noise Orbits laser operating at 1546.52 nm, a 40-GHz 3.8-V V_π EOSpace phase modulator, an a-MZI with a 375-ps path length difference that produces periodic nulls every 2.67 GHz, and a balanced pair of Discovery Semiconductor DSC720s that each have a 20-GHz bandwidth and a responsivity of 0.75 A/W. The a-MZI has voltage controlled temperature stabilization. By observing the current balance on the photodetectors when second-order distortion is minimized, the voltage applied to the a-MZI can be

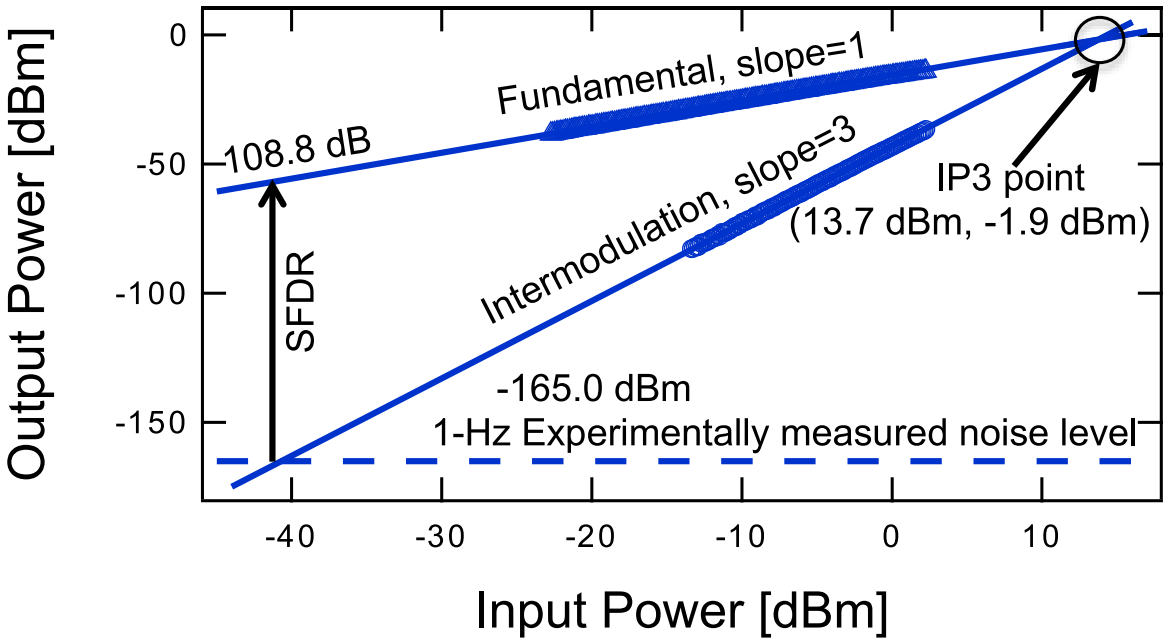

Figure 4.3 The experimentally measured SFDR of the conventional ΦMID link operating at 1.08 mA on each photodiode. The two fundamental tones were at 1.275 and 1.286 GHz. The two third-order intermodulation products were at 1.264 and 1.297 GHz and have a slope of three.

programmatically controlled via a feedback loop to maintain this current balance, effectively holding the a-MZI at quadrature.

For the investigation of the conventional unlinearized link, the photocurrent is maintained at 1.08 mA on each photodiode. The peak gain at 1.29 GHz is -15.5 dB (see Fig. 4.2) and the noise figure was 24.2 dB. These values are within less than 0.5 dB of the theoretically predicted values of –15 dB and 24.4 dB, respectively for this photocurrent and V_π [9]. The slope of the distortion at 1.264 and 1.297 GHz is three, indicating that third-order distortion is dominant. The SFDR is measured to be 108.8 dB in a 1-Hz

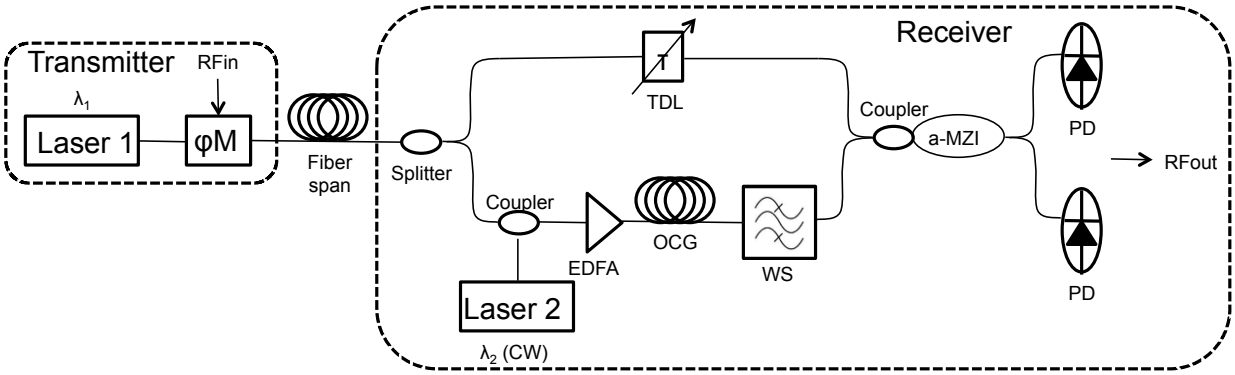

Figure 4.4 Experimental block diagram of the linearized ΦMID link. Lower branch- EDFA: Erbium doped fiber amplifier, OCG: optical comb generator, WS: Waveshaper. Upper branch- TDL: tunable delay line. a-MZI: asymmetric Mach-Zehnder interferometer, PD: photodetector.

bandwidth (see Fig. 4.3), also close to the theoretically predicted value of 109.5 dB.

4.2.2 Third-Order Distortion Free Link

To begin linearizing the link, we add the lower branch to the receiver (see Fig. 4.4). That is, we include a splitter and a combiner prior to the a-MZI. This splits off 30% of the original phase modulated signal, which along with a pump lightwave produced by an NKT laser at a 0.4-nm offset wavelength (1546.92 nm), is amplified and seeds a cascaded four-wave mixing process in the OCG. The EDFA operates at 1.6 W and the OCG consists of three fiber spools. The first spool contains 100-m of highly nonlinear fiber (HNLF) with tension applied in a staircase pattern with ten steps to mitigate stimulated Brillouin scattering [58]. The second spool

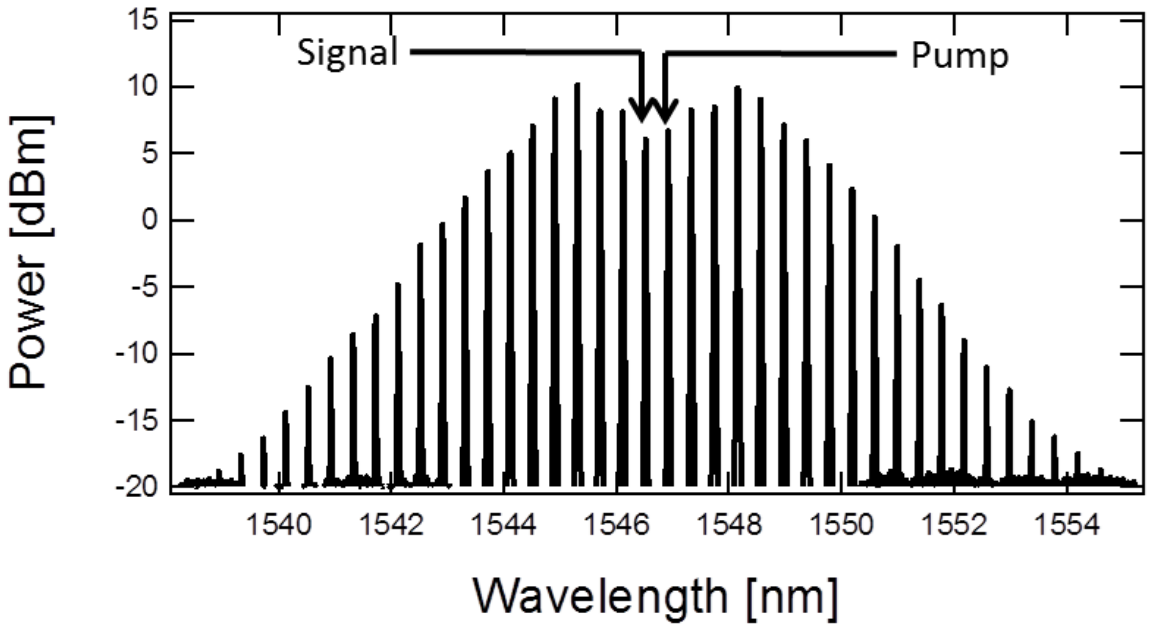

Figure 4.5 The experimentally measured output of the optical comb generator (OCG). The pump and signal lightwaves at 1546.52 and 1546.92 nm, respectively, are injected into the OCG, producing many idlers at equal frequency spacing (0.4 nm) from the pump and signal.

contains 400 m of standard single mode fiber. The third spool contains 160 m of HNLF, also tensioned in a staircase pattern with ten steps. The comb produced by the OCG consists of the original tapped off signal, the pump, and the idlers spaced at equal frequency intervals from the signal and pump (see Fig. 4.5). The phases on the generated idlers are integer multiples of the phase on the original signal. This frequency comb is then sent to a dynamically programmable spectral filter with adjustable attenuation (Finisar Waveshaper). The lightwave with $-3\phi(t)$ modulation at 1548.12 nm is filtered and appropriately attenuated then output. This distortion

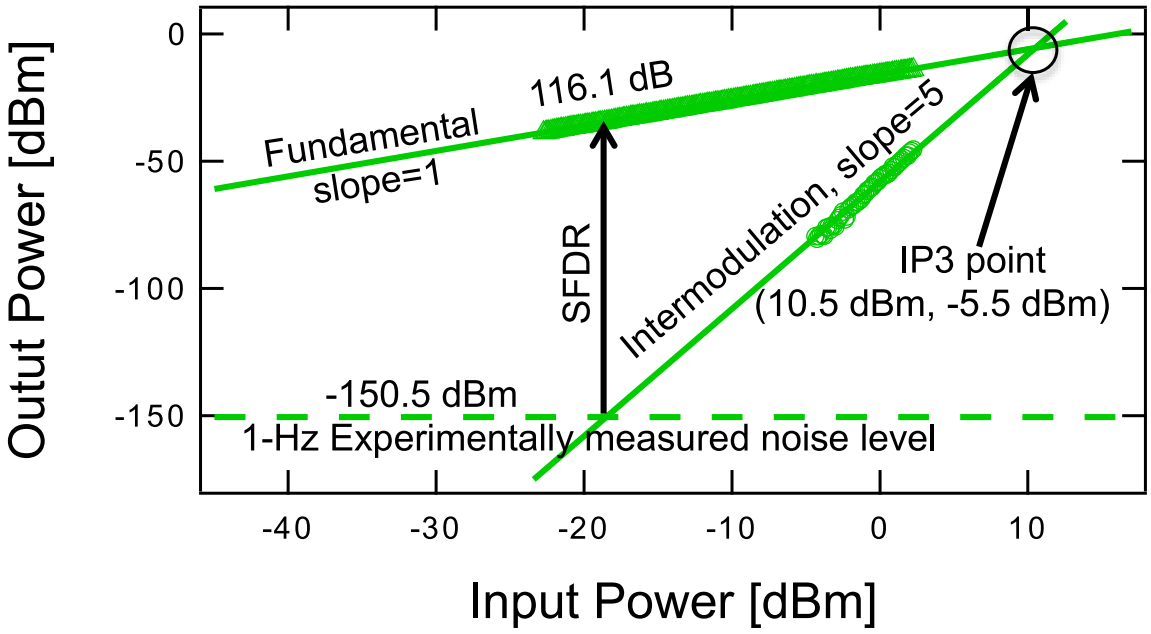

Figure 4.6 The experimentally measured SFDR of the third-order distortion free ($\phi, -3\phi$) link operating at 1.18 mA on each photodiode, with 1.12 mA for ϕ and 0.06 mA for -3ϕ. The two fundamental tones were at 1.275 and 1.286 GHz. The two fifth-order intermodulation products were at 1.264 and 1.297 GHz and have a slope of five

correction lightwave combines with the original lightwave from the upper branch such that the third-order distortion product is fully eliminated from the link. The extinction ratio of the Waveshaper is 50 dB and the pumps in the linearization branch are attenuated to this degree and are thus suppressed so as to not be a significant source of noise.

The long interferometer between the original lightwave (upper branch) and the distortion correction lightwave (lower branch) is path-matched to microwave wavelengths in order to avoid any bandwidth-limiting interference. This is accomplished by taking a group delay measurement for

each path and ensuring they are equal by adjusting the length of standard single-mode optical fiber in the upper branch. The path match is then precisely set using a manually adjusted tunable optical delay. In practice, this delay setting is stable over the course of our measurements and is not actively adjusted.

The total photocurrent present on each photodiode is maintained at 1.18 mA, of which 1.12 mA was from the original phase-modulated lightwave (upper branch) and 0.06 mA was from the $-3\phi(t)$ lightwave (lower branch). This means the $-3\phi(t)$ term is 12.7 dB lower than the original lightwave. By theory we would expect it to be 14.3 dB lower [45]. The discrepancy can likely be attributed to compensation for other sources of third-order distortion in the link, such as the photodiodes. As shown in Fig. 4.6, the measured slope of the intermodulation distortion at 1.264 and 1.297 GHz was five, indicating full-cancellation of third-order distortion and the dominance of fifth-order distortion. The gain is reduced by 0.4 dB relative to the convention unlinearized link to –15.9 dB, where theoretically we would expect the gain to be reduced by 0.5 dB [45]. Finally, we measure an increase in noise figure to 38.7 dB resulting in an SFDR of 116.1 dB in a 1-Hz bandwidth.

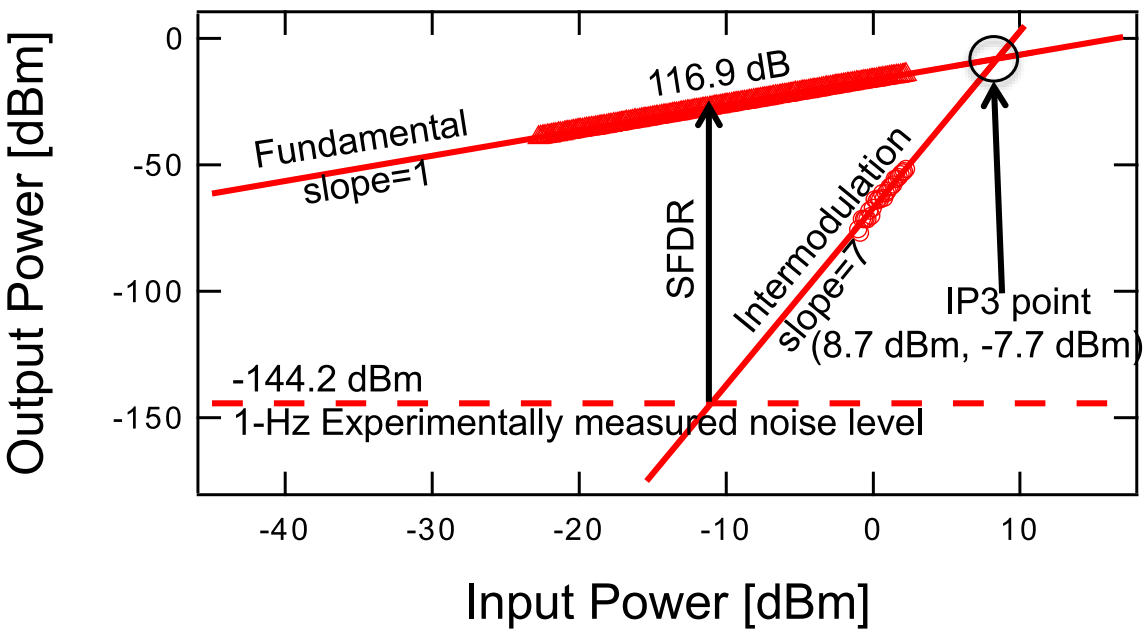

Figure 4.7 The experimentally measured SFDR of the third- and fifth-order distortion free $(\phi, -3\phi, +5\phi)$ link operating at 1.20 mA on each photodiode, with 1.10 mA for ϕ, 0.088 mA for -3ϕ, and 0.010 mA for $+5\phi$. The two fundamental tones were at 1.275 and 1.286 GHz. The two seventh-order intermodulation products were at 1.264 and 1.297 GHz and have a slope of seven.

4.2.3 Third-Order and Fifth-Order Distortion Free Link

To continue linearizing the link, no change to the link setup is required relative to the third-order distortion free link described above. Simply by adjusting the settings of the Waveshaper in software, we can create a more complex filter function that allows both the $-3\phi(t)$ and the $+5\phi(t)$ lightwaves at 1548.12 nm and 1544.92 nm, respectively, to pass. Each of these is independently attenuated and then combined with the original lightwave to simultaneously eliminate both third-order and fifth-order

distortion from the link.

For this final realization, the total photocurrent present on each photodiode is maintained at 1.20 mA, of which 1.10 mA was from the original lightwave, 0.088 mA was from the $-3\phi(t)$ lightwave, and 0.010 mA was from the $+5\phi(t)$ lightwave. Thus the $-3\phi(t)$ term is 11-dB lower than the original lightwave and the $+5\phi(t)$ term is 20.4-dB lower than the 12.6-dB and 24-dB lower, respectively [45]. Again, the slight discrepancies can be attributed to compensation for other sources of distortion in the link. As shown in Fig. 8, the slope of the intermodulation distortion at 1.264 and 1.297 GHz was seven, indicating simultaneous cancellation of both third and fifth-order distortions and the dominance of seventh-order distortion. The gain is reduced by 0.8 dB relative to the conventional unlinearized link to –16.3 dB, where theoretically we would expect the gain to be reduced by 0.7 dB [45]. The noise figure increases to 45 dB resulting in an SFDR of 116.9 dB in a 1-Hz bandwidth (see Fig. 4.7).

4.3 Discussion

In this section we discuss the results in further detail, paying special attention to the bandwidth limitations of this approach and the noise figure of the demonstrated links.

Beyond the bandwidths of the modulator, photodetector, and a-MZI, the system's bandwidth is ultimately limited by the spacing between the

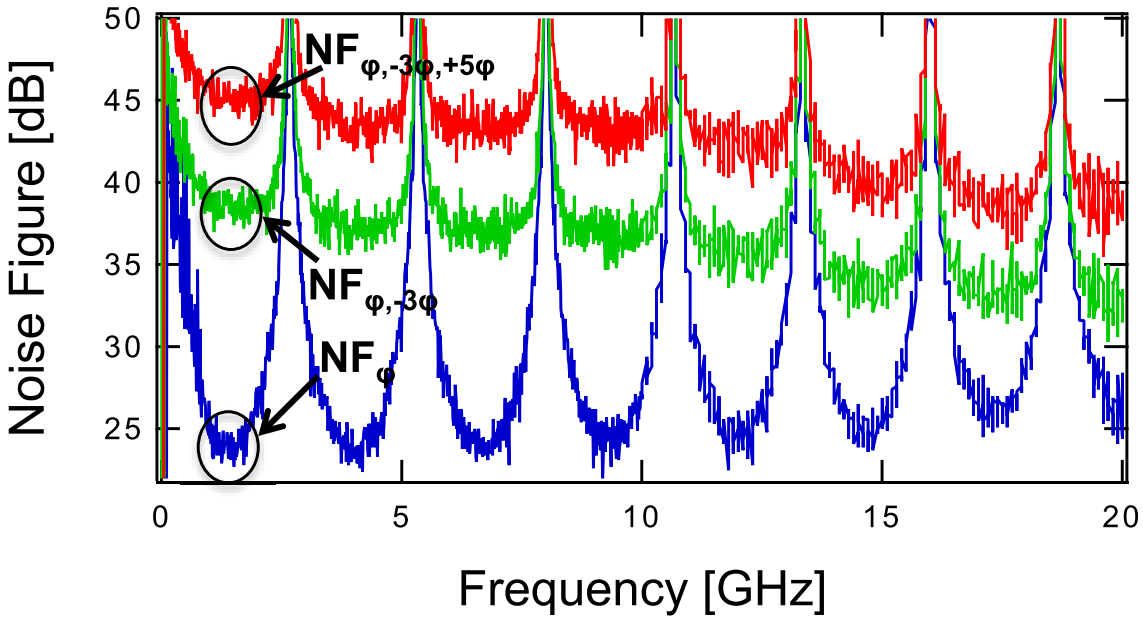

Figure 4.8 Noise figure data for ΦMID link. The blue curve is for the conventional ϕ link, the green is for the $(\phi, -3\phi)$ link, and the red is for the $(\phi, -3\phi, +5\phi)$ link. The black circles show the frequency range of interest for each of the links. The currents are the same as those given in the SFDR plots above. Note the increase in noise figure for each added idler

comb lines. Specifically, the comb line spacing must be greater than the optical bandwidth for each lightwave including the potentially larger optical bandwidth of the higher-order idlers resulting from their greater phase deflection. To increase the maximum link bandwidth, the comb line spacing can be adjusted by choosing a larger wavelength separation between the two lasers. However, this will reduce the number of comb lines available for linearization due to the spectral limitations of the Waveshaper and the gain-bandwidth of the FWM process.

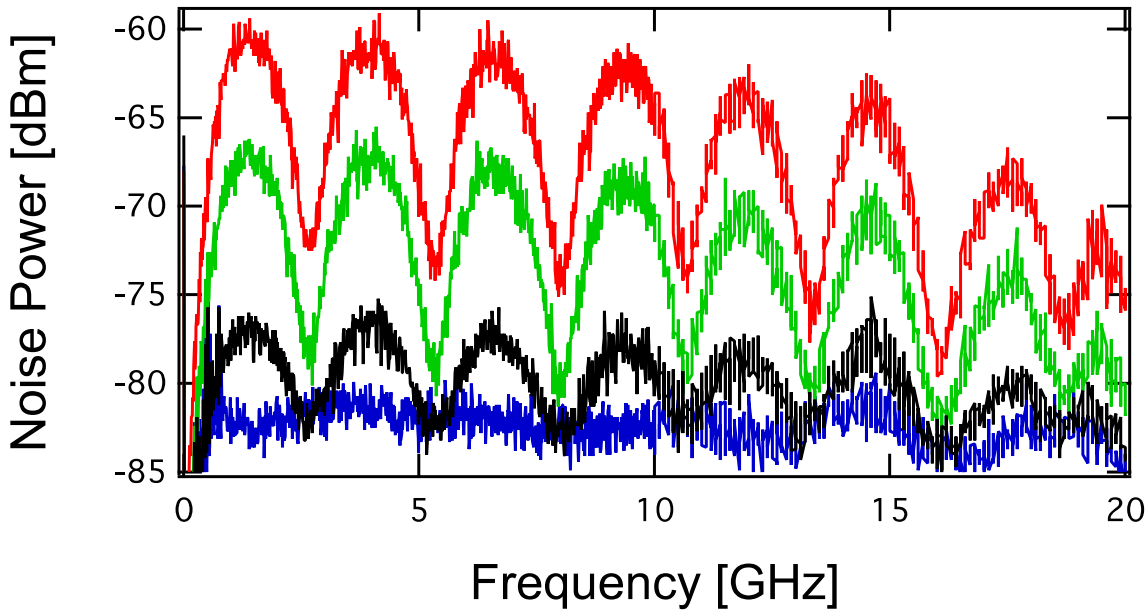

Figure 4.9 Noise power data for ΦMID link. The blue curve is for the conventional ϕ link, the green is for the $(\phi, -3\phi)$ link, and the red is for the $(\phi, -3\phi, +5\phi)$ link. The black curve is the conventional ϕ link with the pump laser instead of the signal laser. Note the increase in noise power in the conventional link going from the signal laser (blue) to the pump laser (black).

While the greater phase deflection of the higher-order idlers produces a larger optical bandwidth and a higher magnitude RF signal, the RF bandwidth remains unchanged. After reception with the a-MZI, distortions arising from intermodulation products that are out-of-band do not matter. Therefore, as long as the a-MZI has sufficient bandwidth to pass the original signal, it will be able to pass the linearized signal formed from the sum of the original and correction signals.

Note that though the SFDR improves with greater number of

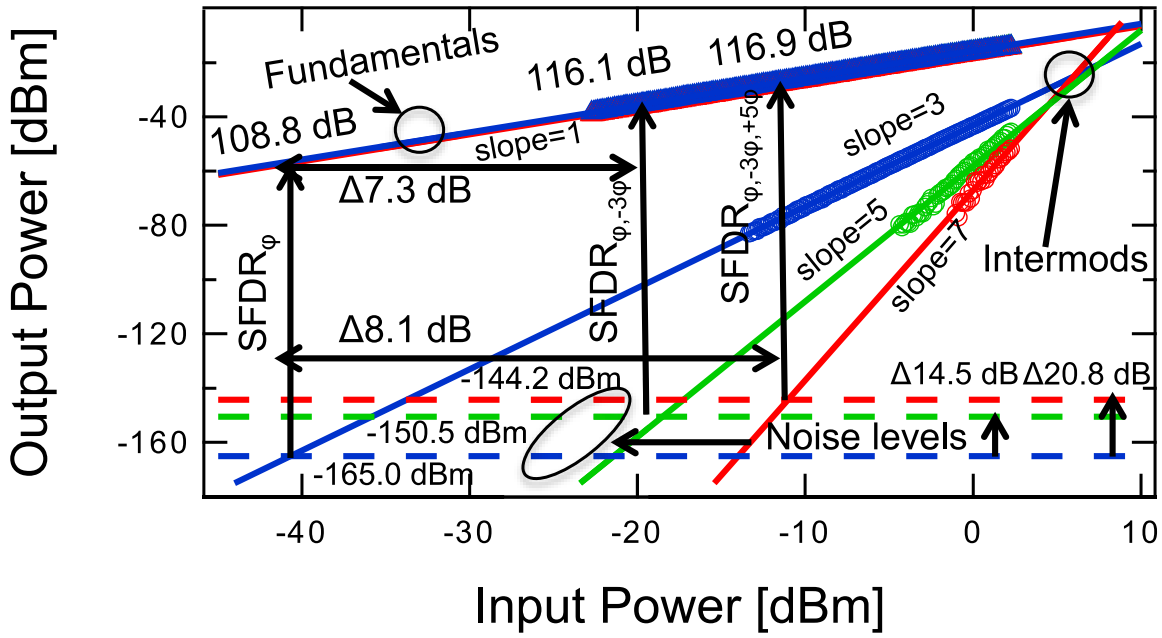

Figure 4.10 Comparison of experimentally measured SFDRs for each of the three links, all operating at about 1 mA on each photodetector. Note the slight degradations in gain (fundamental) and increase in noise level for each additional idler added. Also note the change in slope of the intermodulation product as distortion products are cancelled as well as the 7.3 and 8.1 dB improvement in SFDR despite the increase in noise from the ϕ to the $(\phi, -3\phi)$ link and from the ϕ to the $(\phi, -3\phi, +5\phi)$ link, respectively.

distortion orders cancelled, we observe diminishing returns at a higher rate than predicted due to the significant increase in noise figure with each added linearization term (see Fig. 4.8). Specifically, we measure an SFDR of 116.9 dB in a 1-Hz bandwidth for the third-order and fifth-order distortion free link, however the observed linearization would allow for an SFDR of 134.8 dB in a 1-Hz bandwidth if the link was shot- noise limited.

There are three reasons for the dramatic increase in noise figure

despite the relatively small amount of photocurrent attributable to the added linearization terms. Firstly, the second pump laser that seeds the cascaded FWM process unfortunately has much higher phase noise than the signal laser due to our laser availability (see Fig. 4.9). Secondly, this pump laser is not phase locked to the signal laser [59]. Thirdly, the nonlinear cascaded FWM process amplifies and convolves the phase noises of the two un-locked lasers, with the degree of phase noise amplification increasing with each additional term [59].

These sources of noise degradation immediately suggest two future methods of phase noise mitigation, namely, using a low phase noise laser for the pump and/or phase locking it to the signal laser. Theoretically, phase locking the two lasers should subtract their phase noise and the noise figure increase should be minimal regardless of the number of additional terms included [59]. The phase locking can be achieved by sending a pilot tone from the signal laser with, for example, a tap-off prior to the phase modulation. This would be relatively straightforward for small systems, where there is little physical separation between the transmitter and receiver, such as those involved with signal processing applications. Though not as simple, it could also be accomplished for longer haul systems such as antenna remoting. There is no reason this cannot be done other than limitations of available equipment. Thus, as an exercise, it is instructive to predict the achievable SFDR for the scenario in which the noise figure is not impacted by the added

linearization terms (see Fig. 4.10 for a comparison of SFDRs for each of the links with the measured noise figures). In the case of eliminating third-order distortion, the achievable SFDR would be 127.7 dB instead of 116.1 dB in a 1-Hz bandwidth, an improvement of 11.6 dB over our experimental results or a 19.7-dB total SFDR improvement between the conventional and third-order linearized case. In the case of eliminating both the third-order and fifth-order distortions, the achievable SFDR would be 134.8 dB instead of 116.9 dB in a1-Hz bandwidth, an improvement of 17.9 dB over our experimental results or a 26.8-dB total SFDR improvement between the conventional and the simultaneous third-order and fifth-order linearized case. Indeed, these are impressive SFDRs for such low photocurrents and we hope to experimentally reach these limits in future work through the noise mitigation approaches outlined above.

4.4 Conclusion

In this chapter, we have constructed and tested three links: a conventional unlinearized ΦMID link, a third-order distortion free ΦMID link, and a simultaneous third-order and fifth-order distortion free ΦMID link. We experimentally measure the gain, bandwidth, noise figure, and SFDR for each link and compare to the theoretical values. We observe a minimal degradation (0.4 dB) in gain for each added linearization term that

closely matches to the theoretically predicted values. We experimentally achieve SFDRs of 108.8 dB, 116.1 dB, and 116.9 dB each in a 1-Hz bandwidth for the conventional, third-order distortion free link, and the third-order and fifth-order distortion free link, respectively for approximately 1-mA of current in each photodiode. This is an improvement over the conventional link of 7.3 and 8.1 dB, respectively. To the best of our knowledge, this is the first demonstration of a simultaneous third-order, fifth-order, and all even-order distortion free link in either an intensity or phase modulated architecture. We observe a significant increase in noise figure, attributable in part to the choice of pump laser and lack of phase locking between the lasers, which prevents the realization of the fullest possible improvement in SFDR from the observed degree of linearization. We hope to improve upon these links in the future by implementing noise bandwidth and high power front-end electrical gain systems. In the former case, integration of a high noise level over a mitigation techniques. However, despite the observed noise figure degradation, these links can find application in narrow small bandwidth will still yield a low noise floor. In the latter case, front-end amplification will reduce the impact of the link noise figure to the overall system noise figure.

5 Operational Issues and Mitigation

5.1 Introduction

In this chapter, we explain some of the operational issues with these linearized phase-modulated analog optical links, dividing these into tuning issues and tradeoffs or issues fundamental to the system design. For the latter, we provide potentially methods for mitigation to improve performance beyond that which we have experimentally demonstrated.

5.2 Tuning Issues

In this section, we examine three tuning issues relevant to the operation of the linearized phase modulated link including relative optical pump polarizations and powers, bias maintenance of the a-MZI, and path length matching in the large interferometer consisting of the conventional and linearized branches.

The efficiency of the FWM conversion process is heavily dependent on the relative optical pump polarizations and powers. That is, small relative differences between the polarizations of the two lasers and their optical powers at the input to the HNLF can have large effects on the shape, number, wavelength range, and intensities of the generated comb lines.

Fortunately, however, once these polarizations and powers are set, they require only occasional adjustment.

The a-MZI consists of one optical input, two optical outputs, and one voltage input. The voltage controls a thermo-electric Peltier cell within the a-MZI that, when heated or cooled, changes the power balance between the two optical outputs. Due to drift, this voltage must be constantly monitored and adjusted in order to maintain the desired quadrature bias point, similar to maintaining the bias of an MZM. One way this can be accomplished is to use a bias board which taps off a small percentage of the input optical power and a small percentage of one or both arms of the output optical power, then dynamically changes the voltage output to achieve the desired optical power ratio. In our experiments we programmatically read the photodetector currents from the DC power supply, generate an error signal, and use an algorithm to tune the bias voltage.

There is a phase walk-off issue caused by the relative path length difference in the large interferometer consisting of the conventional branch in one arm and the linearization branch in the other. The system bandwidth is the intersection of the bandwidths of the a-MZI and the large interferometer. In the best case scenario, this is the a-MZI bandwidth as the large interferometer should ideally present no bandwidth limitations if both arms are exactly path matched. The lengths can be measured by finding the group delay through each path. Coarse adjustments can be made by adding or

removing fiber from the paths. Fine tune adjustments can be made with one or more tunable optical delay lines in one or both paths. However, the lengths can only be measured accurately up to the group delay resolution limit of the instrument, which places an upper limit on the length of fiber in each arm. An optical time-domain reflectometer may be used to overcome this limitation. In addition to the static length differences, it is possible to have small relative variances due to, for example, unequal thermal expansion or contraction of the fiber lengths between the two paths. While inconsequential for low frequency microwave signals, it can become a severe issue for high frequency signals as the path length matching must be valid for microwave frequency accuracy. This slow, small length drift can potentially be taken care of with a feedback loop.

5.3 Fundamental Limits and Tradeoffs

In our experiment we have two free running CW lasers. The first one is a low phase noise laser that carries the fundamental signal through the conventional branch. The second is a higher noise laser that, together with a portion of the first laser, seeds the FWM process from which the linearization terms are filtered. Phase noise adds directly with the phase-modulated signal and the nonlinear cascaded FWM process amplifies and convolves the phase noises of the two un-locked lasers, with the degree of phase noise

amplification increasing with each additional term. A simple way to improve the link is to replace the second laser with a low phase noise laser similar to the first laser. However, because they are still not locked together, improvement in noise figure would still be limited by the uncorrelated phase noise. Here we present three methods for locking the lasers together.

One method is to use an optical phase locked loop. In this method, a portion of the first laser is tapped off prior to modulation and sent to the receiver. By coupling this with the second laser and beating them at a photodetector, we can generate an error signal to drive the second laser. The locking bandwidth would be limited by the total loop length, which is dominated by the fiber length between the transmitter and receiver. Therefore, this solution would work for low lengths links, systems in which the transmitter-receiver distance was small.

The other two methods start with a single laser. By injection locking a master laser to two slave lasers, each of which is fed to one branch, two phase locked lasers can be used. The last method involves driving a modulator with a microwave signal at half the comb line spacing in a dual sideband suppressed carrier configuration. The separation between the two sidebands adjacent to carrier is then the optical comb line spacing. We can optically filter these and feed one to each path. Notice in all three methods, a second fiber span is required between the transmitter and receiver. This partially mitigates one of the advantages of a phase modulated link, which is the

ability to have balanced detection without running a dual fiber span. However, the requirement is less burdensome than for an intensity modulated link having balanced detection because the two fiber lengths do not have to be path matched. In chapter four we go into detail about potential improvements to SFDR if we are able to completely eliminate phase noise.

In addition to the normal bandwidth constraints imposed by the devices (modulator, detector, and a-MZI), there are additional constraints imposed by the linearization system that depend on the microwave frequency of operation, the dynamic range, the optical comb line spacing, and the number of linearization terms used (i.e. degree of linearization). To understand this tradeoff, imagine two comb lines, one of which is phase-modulated with the microwave signal and the other which is the second CW pump laser, spaced at a frequency $\boldsymbol{\Delta f_{comb}}$ apart. After the FWM process, more comb lines appear at optical frequencies that are linear combinations of the two pump frequencies (essentially at integer multiples of $\boldsymbol{\Delta f_{comb}}$ above and below the two pumps). Additionally, the phases of the comb lines are also linear combinations of the two pump phases. Therefore, higher order comb lines (those further from the pump) have greater phase amplification. For the deflection of each linearization term to fit within the comb line spacing, its bandwidth must not interfere (overlap) with those of its immediate neighbors'. The neighbor furthest away from the pump possesses

the greatest phase deflection and thus places a constraint on the highest order linearization term that can be used.

As the comb line spacing increases, the number of practically usable linearization terms is further limited by the gain bandwidth of the FWM process, which extends throughout the C-band and into the L-band, or more likely the bandwidth of the programmable spectral filter, whichever is lower.

5.4 Summary and Conclusion

We have explained some of the issues associated with operating these linearized phase-modulated links. In particular, we went over tuning issues including polarization and power matching in the optical pumps, bias voltage maintenance in the a-MZI, and phase walkoff issues associated with path length mismatches in the large interferometer. We also covered fundamental issues and tradeoffs relating to uncorrelated phase noise in the two lasers and tradeoffs between microwave frequency of operation, dynamic range, comb line spacing, and number of linearized terms. Where possible we have offered solutions to mitigate those issues not fundamental to the system design.

6 Microwave Function Generation

6.1 Introduction

In this chapter we demonstrate a microwave function generator based on precisely engineering the distortion in a microwave photonic link. By distorting a 5-GHz sinusoid we are able to generate a 5-GHz triangle wave and square pulse train.

Efficient microwave generation of high frequency waveforms is becoming increasingly critical to many commercial and military applications, including next-generation bit-error-rate measurement systems and optical analog and digital communications [1]. In addition, microwave function generators are essential components of electronic test equipment, used to create waveforms for fault detection and failure and reliability analysis in a device under test. Most commercial function generators interpolate between target voltage levels using digital signal processing techniques and as such, are limited in their bandwidth due to a fundamental tradeoff between transistor speed and dynamic range [2]. Current products can only simulate signals in the low GHz range [3]. Here we introduce a photonically-enabled analog method exploiting the nonlinear optical process of cascaded four-wave mixing to accomplish function generation without the stringent bandwidth limitations presented by electronic systems.

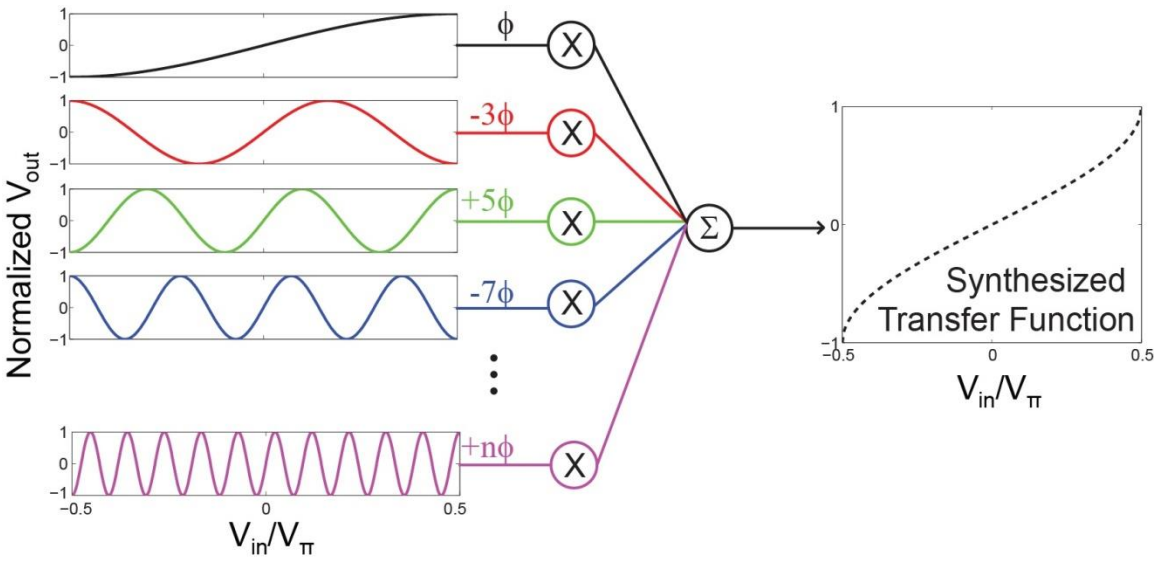

Figure 6.1 In this example, an arcsine transfer function is synthesized to produce a triangle wave output for a sine wave input.

6.2 Method

To enable generation of user defined functions from input sinusoids we tailor the transfer function (input voltage to output voltage) of a microwave photonic link [4]. To synthesize a user defined transfer function we exploiting the integer phase relationships of the comb lines created in a cascaded four-wave mixing process [5] and appropriately filter and scale the desired components in a pulse shaper as depicted in Fig. 6.1. We begin by first defining a target periodic waveform we wish to generate and then defining the transfer function required to convert between an input sinusoid and the desired waveform at the same microwave frequency. Knowledge of our transfer function allows us to determine both the Fourier components

necessary to construct it as well as their respective coefficients. This can be done immediately if the Fourier components are well known or easily calculatable or it can be back-calculated from the Taylor series.

To further elucidate our approach, we work through the simple example of the first two components of a triangle (or ramp) wave. First, we recognize that in order to create a triangle wave output from a sinusoidal input, we must create an arcsin transfer function. Then, we find the first two terms of the Taylor expansion of an arcsin. Finally we use the first two terms of the Taylor expansion of sin(x) and a scaled sin(3x) to find the value of the scaling factor knowing what the ratio between the first and third powers of the Taylor expansion of the arcsin should be. With a greater number of terms, a matrix inversion technique can be used to find the scaling factors for each term. These scaling factors can then be applied to the respective Fourier components and summed together to synthesize the desired transfer function (see Fig. 6.1). The method is a generalization of that described in the appendix of [4], where the scaling factors are found such that the higher order terms are no longer zero but instead some target value. Whereas in our previous work [4] the goal was to linearize a link by eliminating distortion, here we intentionally add distortion to produce a transfer function that will give us the desired microwave waveform. This is an analog process and the waveform quality is primarily limited by the photodetector bandwidth.

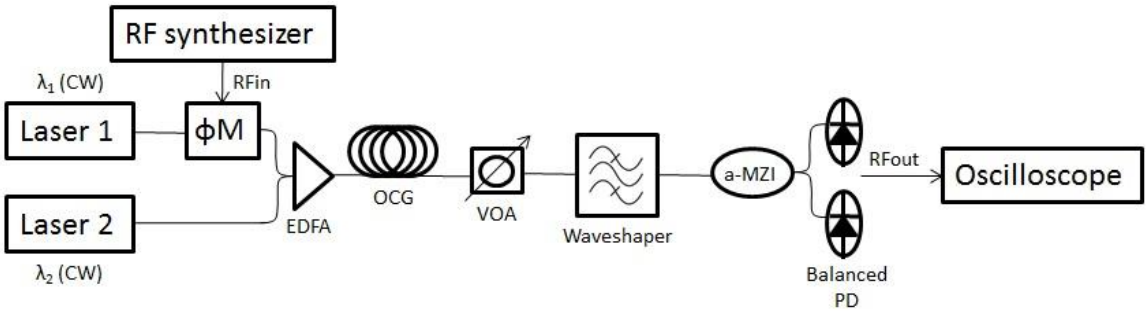

Figure 6.2 Experimental block diagram of the arbitrary waveform generator. CW: continuous wave, ΦM: phase modulator, EDFA: Erbium doped fiber amplifier, OCG: optical comb generator, VOA: variable optical attenuator, a-MZI: asymmetric Mach-Zehnder interferometer, PD: photodiode.

6.3 Experiment

In our experiment (see Fig. 6.2), we combine two CW pump lasers spaced 0.4 nm apart after phase modulating one of them, the amplify them and send them through a cascaded four-wave mixing based optical comb generator (OCG) consisting of a series of tensioned highly nonlinear fiber, single mode fiber, and untensioned highly nonlinear fiber [6]. The cascaded four-wave mixing interaction inside the OCG produces equally spaced comb lines on either side of the two pump lasers whose phases are uniquely determined by those of the pump lasers. In fact, because only one of the pump lasers is phase modulated, these phases are integer multiples of the modulated pump phase. All of these comb lines are then sent to a pulse shaper (Finisar Waveshaper), which is programmed to filter and attenuate

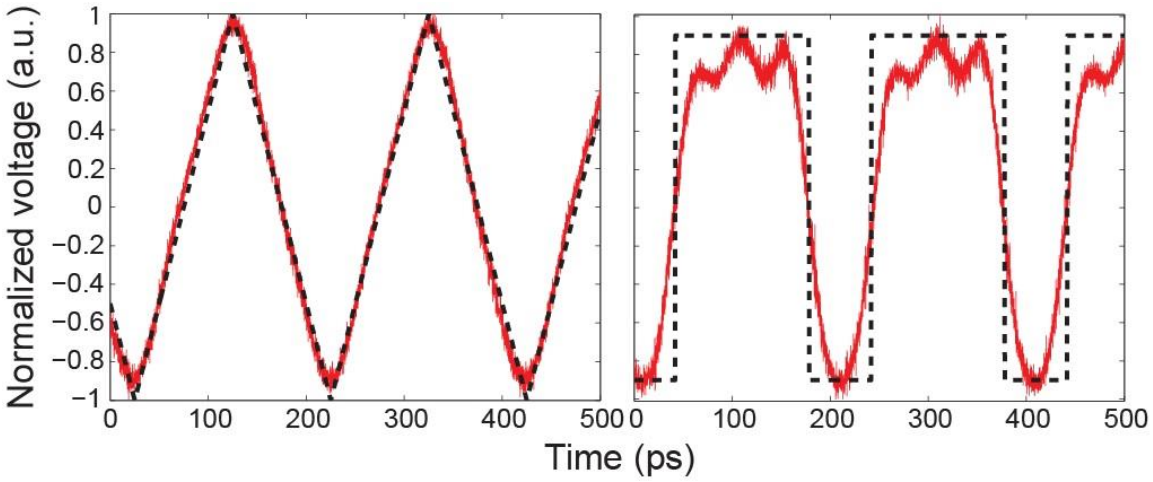

Figure 6.3 Experimental results in red, target waveforms in dotted black, left: triangle wave, right: square pulse, both at 5 GHz.

the appropriate are then interferometrically detected at the asymmetric Mach-Zehnder and combined in a 26-GHz balanced photodetector. The resulting waveforms are shown in red in Fig. 6.3 with the ideal waveforms superimposed in dotted black. The left plot is the generated triangle wave and the right plot is the generated square pulse wave. Note that the generated triangle wave approximates the ideal triangle wave very well whereas, for the square wave the Fourier sum for the needed transfer function converges more slowly.

7 Conclusion

In this thesis we introduced a novel method for distortion elimination in phase-modulated microwave photonic links. Our method is unique in that it accomplishes the linearization entirely in the optical domain, something that has not been done before. We provided a short background in microwave photonics and nonlinear optics and then detailed the theory of operation for our method. Next we described our architecture and went over our experimental results, validating the method. We discussed the operational issues, limitations, and tradeoffs of our design. Finally, we applied our method to another area of microwave photonics, function generation, and provided a design and experimental results. Undoubtedly the intersection between microwave photonics and nonlinear optics possesses many other rich, interesting, and fruitful applications that have yet to be discovered.

Bibliography

[1] A. J. Seeds and K. J. Williams. (2006). Microwave photonics. *J. Lightwave Technol. 24(12)*, pp. 4628–4641.

[2] J. Yao. (2012). A tutorial on microwave photonics. *IEEE Photonics society newsletter. 26(2)*, pp. 4–12.

[3] J. Capmany and D. Novak. (2007). Microwave photonics combines two worlds. *Nat. Photonics. 1(6)*, pp. 319–330.

[4] J. Yao. (2009). Microwave photonics. *J. Lightwave Technol. 27(3)*, pp. 314–335.

[5] W. S. Chang, ed., *RF Photonic Technology in Optical Fiber Links*. Cambridge University, 2002.

[6] V. J. Urick, J. D. McKinney, and K. J. Williams, *Fundamentals of Microwave Photonics*. John Wiley & Sons, 2015.

[7] R. H. Walden. (1999). Analog-to-digital converter survey and analysis. *IEEE Journal on selected areas in communications 17(4),* pp. 539-550.

[8] G. C. Valley. (2007). Photonic analog-to-digital converters. *Optics Express 15*(5), pp. 1955-1982.

[9] V. Urick, F. Bucholtz, P. Devgan, J. McKinney, and K. Williams. (2007). Phase modulation with interferometric detection as an alternative to intensity modulation with direct detection for analog-photonic links. *IEEE Trans. Microw. Theory Tech. 55(9)*, pp. 1978–1985.

[10] C. H. Cox III, E. Ackerman, G. Betts, and J. Prince. (2006). Limits on the performance of RF-over-fiber links and their impact on device design. *IEEE Transactions on Microwave Theory and Techniques, 54(2)*, 906-920.

[11] J. B. Johnson. (1928). Thermal agitation of electricity in conductors. *Physical review 32(1)*, pp. 97.

[12] H. Nyquist. (1928). Thermal agitation of electric charge in conductors. *Physical review 32(1)*, pp. 110.

[13] H. A. Haus, *Electromagnetic noise and quantum optical measurements*. Springer Science & Business Media, 2012.

[14] W. Schottky. (1918). Regarding spontaneous current fluctuation in different electricity conductors. *Annalen der Physik 57(23)*, pp. 541-567.

[15] A. Vilcot, B. Cabon, and J. Chazelas, eds., *Microwave Photonics: from Components to Applications and Systems*. Springer, 2003.

[16] C. Rumelhard, C. Algani, and A. Billabert, *Microwaves Photonic Links: Components and Circuits*. John Wiley & Sons, 2011.

[17] B. Wilson, Z. Ghassemlooy, and I. Darwazeh, eds., *Analogue Optical Fibre Communications*. ITE, 1995.

[18] C. H. Cox III, *Analog Optical Links: Theory and Practice*. Cambridge University, 2006.

[19] R. C. Williamson and R. D. Esman. (2008). RF photonics. *Journal of Lightwave Technology, 26(9)*, 1145-1153.

[20] C. H. Cox III, E. Ackerman, and G. Betts, "Relationship between gain and noise figure of an optical analog link," in *IEEE MTT-S International Vol. 3 Microwave Symposium Digest*, San Francisco, CA, 1996, pp. 1551-1554.

[21] W. K. Burns, M. M. Howerton, and R. P. Moeller. (1999). Broad-band unamplified optical link with RF gain using a LiNbO 3 modulator. *IEEE Photonics Technology Letters 11(12)*, pp. 1656-1658.

[22] E. Ackerman, G. Betts, W. Burns, J. Campbell, C. H. Cox III, N. Duan, J. Prince, M. Regan, and H. Roussell, "Signal-to-noise performance of two analog photonic links using different noise reduction techniques" in *IEEE MTT-S International Microwave Symposium*, Honolulu, HI, 2007, pp. 51-54.

[23] E. Ackerman, S. Wanuga, D. Kasemset, A. S. Daryoush, and N. Samant. (1993). Maximum dynamic range operation of a microwave external modulation fiber-optic link. *IEEE Transactions on Microwave Theory and Techniques, 41(8)*, 1299-1306.

[24] M. J. LaGasse, W. Charczenko, M. C. Hamilton, and S. Thaniyavarn. (1994). Optical carrier filtering for high dynamic range fibre optic links. *Electronics Letters 30(25)*, pp. 2157-2158.

[25] D. Marpaung, C. Roeloffzen, and W. van Etten, "A novel modulation scheme for noise reduction in analog fiber optic links" in *Proceedings Symposium IEEE/LEOS Benelux Chapter*, 2005.

[26] E. Ackerman and C. H. Cox III, "Microwave photonic links with gain and low noise figure," in *Lasers and Electro-Optics Society*, 2007, pp. 38-39.

[27] S. A. Maas, *Nonlinear Microwave Circuits*. Artech House, 1988.

[28] R.B. Childs and V.A. O'Byrne, "Multichannel AM video transmission using a high-power Nd:YAG laser and linearized external modulator," IEEE J. Sel. Area. Comm. **8**(7), 1369-1376 (1990).

[29] R. Sadhwani and B. Jalali, "Adaptive CMOS predistortion linearizer for fiber-optic links," J. Lightwave Technol. **21**(12), 3180-3193 (2003).

[30] R.M. de Ridder and S.K. Korotky, "Feedforward compensation of integrated optic modulator distortion," Technical Digest Conference Optical Fiber Communication, San Francisco, CA, 1990, paper WH5.

[31] S.R. O'Connor, T.R. Clark Jr., and D. Novak, "Wideband adaptive feedforward photonic link," J. Lightwave Technol. **26**(15), 2810-2816 (2008).

[32] P. Li, R. Shi, M. Chen, H. Chen, S. Yang, and S. Xie, "Linearized photonic IF downconversion of analog microwave signals based on balanced detection and digital signal post-processing," 2012 IEEE International Topical Meeting on Microwave Photonics pp. 68-71 (2012).

[33] D. Lam, A. Fard, B. Buckley, and B. Jalali, "Digital broadband linearization of optical links," Opt. Lett. **38**(4), 446-448 (2013).

[34] T.R. Clark, S.R. O'Connor, and M.L. Dennis, "A phase-modulation I/Q-demodulation microwave-to-digital photonic link," IEEE Trans. Microw. Theory Tech. **58**(11) 3039-3058 (2010).

[35] T.R. Clark and M.L. Dennis, "Coherent optical phase-modulation link." IEEE Photon Technol. Lett. **19**(16), 1206-1208 (2007).

[36] L.M. Johnson and H. V. Roussell, "Reduction of intermodulation distortion in interferometric optical modulators," Opt. Lett. **13**(10), 928-930 (1988).

[37] S.K. Korotky and R.M. de Ridder, "Dual parallel modulation schemes for low-distortion analog optical transmission," IEEE J. Sel. Area. Comm. **8**(7), 1377-1381 (1990).

[38] G. Betts, " Linearized modulator for suboctave-bandpass optical analog links," IEEE Trans. Microw. Theory Tech. **42**(12), 2642-2649 (1994).

[39] W.B. Bridges and J.H. Schaffner, "Distortion in linearized electrooptic modulators," IEEE Trans. Microw. Theory Tech. **43**(9), 2184-2197 (1995).

[40] M. Huang, J. Fu, and S. Pan, "Linearized analog photonic links based on a dual-parallel polarization modulator," **37**(11), 1823-1825 (2012).

[41] B.M. Haas and T.E. Murphy, "A simple, linearized, phase-modulated analog optical transmission system," IEEE Photon. Technol. Lett. **19**(10), 729-731 (2007).

[42] J.D. McKinney, K. Colladay, and K.J. Williams, "Linearization of phase-modulated analog optical links employing interferometric demodulation," J. Lightwave Technol. **27**(9), 1212-1220 (2009).

[43] J. D. McKinney and K. J. Williams, "A linearized phase-modulated analog optical link," in *CLEO: QELS_Fundamental Science*, May 2008, pp. CMP4.

[44] B. M. Haas, V. J. Urick, J. D. McKinney, and T. E. Murphy. (2008). Dual-wavelength linearization of optically phase-modulated analog microwave signals. *Journal of Lightwave Technology 26(15)*, pp. 2748-2753.

[45] A. Bhatia, H. Ting, and M.A. Foster. (2014). Linearization of phase-modulated analog optical links using a four-wave mixing comb source. *Optics Express 22(25)*, pp. 30899-30909.

[46] A. Bhatia, H. Ting, and M.A. Foster. (2016). All-Optical Multi-Order Distortion Elimination in a Phase-Modulated Microwave Photonic Link. *Journal of Lightwave Technology*.

[47] R. W. Boyd, *Nonlinear Optics*. Academic Press, 1992.

[48] P. A. Franken, A. E. Hill, C.W. Peters, and G. Weinreich. (1961). Generation of optical harmonics. *Physical Review Letters 7(4)*, pp. 118.

[49] G. Agrawal, *Nonlinear Fiber Optics*. Academic Press, 2013.

[50] E.P. Ippen and R.H. Stolen. (1972). Stimulated Brillouin scattering in optical fibers. *Applied Physics Letters 21(11)*, pp. 539-541.

[51] I. Andonovic and D. Uttamchandani, *Priciples of Modern Optical Systems*. Artech House, 1989.

[52] J.M. Boggio, J.D. Marconi, and H.L. Fragnito. (2005). Experimental and Numerical Investigation of the SBS-Threshold Increase in an Optical Fiber by Applying Strain Distributions. *Journal of Lightwave Technology 23(11)*, pp. 3808-3814.

[53] B. Saleh and M. Teich, *Fundamentals of Photonics, 2nd ed*. Wiley and Sons, 2007.

[54] M. Abramowitz and I. Stegun, *Handbook of Mathematical Functions with Formulas, Graphs, and Mathematical Tables*. Dover, 1965.

[55] H Chi, X Zou, J Yao. (2009). "Analytical models for phase-modulation-based microwave photonic systems with phase modulation to intensity modulation conversion using a dispersive device." Journal of Lighwave Technology, pp. 511-521.

[56] J. Kakande, R. Slavik, F. Parmigiani, A. Borgis, D. Syvridis, L. Gruner-Nielsen, R. Phelan, P. Petropoulos, and
D. Richardson, "Multilevel quantization of optical phase in a novel coherent parametric mixer architecture," Nat. Photonics 5(12), 748-752 (2011).

[57] E. Myslivets, B. P. Kuo, N. Alic, and S. Radic. (2012). Generation of wideband frequency combs by continuous-wave seeding of multistage mixers with synthesized dispersion. *Optics Express 20(3)*, pp. 3331–3344.

[58] T. Hasegawa, K. Inoue, and K. Oda. “Polarization independent frequency conversion by fiber four-wave mixing with a polarization diversity technique,” IEEE Photon. Technol. Lett. 5(8), 947-949 (1993).

[59] Z. Tong, A. Wiberg, E. Myslivets, B. Kuo, N. Alic, and S. Radic. (2012). Spectral linewidth preservation in parametric frequency combs seeded by dual pumps. *Optics Express 20(16)*, pp. 17610-17619.

[60] R. Ziemer and W. H. Tranter, *Principles of Communications: Systems, Modulation, and Noise*. Wiley and Sons, 2006.

Biographical Sketch

Amit Bhatia was born and raised in southern California and completed his Bachelor's degree in electrical engineering at the University of Southern California. He worked in the satellite industry for several years before beginning graduate school at Johns Hopkins University in Baltimore, MD where he completed his doctoral work in microwave photonics.